Heating-induced drag reduction in relative movement of parallel plates

J. M. Floryan, S. Shadman, and M. Z. Hossain
Department of Mechanical and Materials Engineering, University of Western Ontario, London, Ontario, N6A5B9, Canada

(Received 10 February 2018; published 4 September 2018)

An external force is required to maintain the relative movement of horizontal plates. It is shown that this force is reduced when the plates are subject to a spatially distributed heating. The largest reduction occurs for heating wavelengths of the order of distance between the plates with its magnitude increasing proportionally to the second power of the relevant Rayleigh number. It is shown that a sufficiently strong heating eliminates the need for the driving force altogether. The drag-reducing effect is active only in small Reynolds number flows and is stronger in fluids with smaller Prandtl numbers.

DOI: 10.1103/PhysRevFluids.3.094101

I. INTRODUCTION

Friction between moving shafts found in numerous machines contributes to the energy cost of operating these devices. This cost may be estimated by determining force required to maintain the relative motion between these parts. Similar processes can be found in other applications, e.g., the towing of a free-floating body in a shallow basin. In general, flows which form in the space between two infinite plates in relative motion are well approximated by the Couette flow model, which is one of the family of simple flows frequently used in analyses.

Couette flow is characterized by the absence of a streamwise pressure gradient, a linear velocity distribution across the fluid layer and the lack of the linear stability limit [1]. The nonlinear stability analyses are well reviewed in Ref. [2] and demonstrate various routes to secondary finite-amplitude states as well as to turbulence. Surface modifications either in the form of transverse grooves [3], axisymmetric ribs [4], or wall transpiration [5] can lead to centrifugal instabilities. Replacing the plane Couette flow with the annular Couette flow leads to shear instabilities [6]. Transition to secondary states leads to an increase in the wall shear and the need to increase the externally imposed driving force. Such states should be avoided if minimization of energy cost is of interest.

Analyses of nonisothermal Couette flows are rather limited. They typically involve fluids with temperature-dependent material properties in a flow system exposed to a spatially uniform heating [7]. The addition of gravity brings in buoyancy effects which may generate secondary flows through the Rayleigh-Bénard instability [8,9] if the relevant critical conditions are met. Analyses of the resulting mixed convection are well reviewed in Ref. [10]. The use of spatially nonuniform heating leads to structured convection which occurs regardless of the heating intensity, but which is yet to be studied in the case of Couette flow. It is known that such heating leads to the reduction of pressure losses in pressure-gradient driven flows [11–13].

The present work is part of a wider search for drag-reducing methods which, in the present case, manifests itself in the form of reduction of the external force required to maintain the relative plate movement. One of the approaches is to ensure stability of the flow so that transition to secondary states is avoided. Another approach, which is followed here, is to create spatial flow modulations which could lead to the reduction of shear and, thus, reduction of the driving force. The use of grooves for this purpose has been explored in Refs. [14–16]. This paper explores modulations created by spatially distributed heating. Since convective flows are highly unstable, we shall limit this analysis

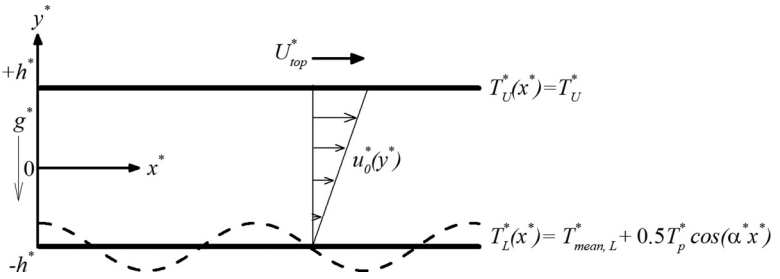

FIG. 1. Schematic diagram of the flow system.

to conditions when secondary flows are not likely to form. Precise determination of heating conditions resulting in a system bifurcation requires a formal stability analysis and such analysis will not be attempted. Results of stability analysis of convection between stationary plates [17,18] provides a good guidance for selection of acceptable heating levels. Analysis of stability of pressure-gradient-driven flow in a periodically heated channel shows flow stabilization with an increase of the flow Reynolds number [19] which suggests that estimates taken from Refs. [17,18] are valid for the flow driven by the moving plate. Section II presents the model problem where the lower plate is heated, and the upper plate is kept isothermal. Section III provides a description of the system dynamics. Section III A discusses the response to a spatially periodic heating while the mean temperatures of the plates are kept the same. Since it is unlikely that the mean temperatures can remain identical in applications, Sec. III B discusses changes in the system response due to a mismatch between these temperatures. Section III C describes variations of the system response due to changes of the Prandtl number. Section IV discusses the heat transfer processes. Section V describes the system response when the upper plate is heated while the lower plate is isothermal. Section VI provides a short summary of the main conclusions.

II. PROBLEM FORMULATION

Consider two horizontal plates moving relative to each other and separated by a distance $2h^*$ as shown in Fig. 1. The resulting gap extends to $\pm\infty$ in the x direction and is filled with a fluid of thermal conductivity k^*, specific heat c^*, thermal diffusivity $\kappa^* = k^*/\rho^* c^*$, kinematic viscosity ν^*, dynamic viscosity μ^*, thermal expansion coefficient Γ^* and with variations of density ρ^* described by the Boussinesq approximation. The gravitational acceleration g^* acts in the negative y direction. The upper plate is pulled in the positive x direction with a constant velocity $U^*_{\rm top}$ while the lower plate is stationary. When the system is isothermal, the drag force and the resulting flow field can be easily determined,

$$\boldsymbol{v}_0(x, y) = [u_0(y), 0] = \left[\frac{(1+y)}{2}, 0\right], \quad p_0(x, y) = C, \quad Q_0 = 1, \quad \tau_0 = -0.5, \quad F_0 = 0.5, \tag{2.1}$$

where velocity has been scaled with $U^*_{\rm top}$ as the velocity scale, Q_0 stands for the flow rate scaled with the same velocity scale, τ_0 stands for the shear acting on the upper plate scaled with $U^*_{\rm top}\mu^*/h^*$, F_0 denotes the force per unit length and width required to drag the upper plate scaled with $U^*_{\rm top}\mu^*/h^*$ and the relevant Reynolds number is defined as $\mathrm{Re} = U^*_{\rm top} h/\nu$.

Introduce an external heating resulting in sinusoidal temperature variations along the lower plate,

$$T^*_L(x^*) = T^*_{{\rm mean},L} + 0.5\, T^*_p \cos(\alpha^* x^*), \quad T^*_U(x^*) = T^*_U, \tag{2.2a,b}$$

where the subscripts "*mean*" and "p" refer to the mean and periodic parts, respectively, T^*_p is the peak-to-peak amplitude of the periodic component, and subscripts L and U refer to the lower and upper plates, respectively. Using the upper plate's temperature for reference and introducing the

relative temperature $\theta^* = T^* - T_U^*$ lead to plates' temperatures of the form

$$\theta_L^*(x) = \theta_{\text{uni}}^* + 0.5\,\theta_p^* \cos(\alpha^* x^*), \quad \theta_U^*(x) = 0, \tag{2.3}$$

where $\theta_{\text{uni}}^* = T_{\text{mean,L}}^* - T_U^*$, $\theta_p^* = T_p^*$. Using half of the gap height h^* as the length scale and $\kappa^*\nu^*/(g^*\Gamma^* h^{*3})$ as the temperature scale results in the temperature boundary conditions of the form

$$\theta_L(x) = \text{Ra}_{\text{uni}} + 0.5\,\text{Ra}_p \cos(\alpha x), \quad \theta_U(x) = 0, \tag{2.4}$$

where $\text{Ra}_{\text{uni}} = g^*\Gamma^* h^{*3} T_{\text{uni}}^*/(\kappa^*\nu^*)$ is the uniform Rayleigh number measuring the intensity of the uniform heating, $\text{Ra}_p = g^*\Gamma^* h^{*3} T_p^*/(\kappa^*\nu^*)$ is the periodic Rayleigh number measuring the intensity of the periodic heating, and all material properties are evaluated at the reference temperature T_U^*.

The field equations take the form

$$\frac{\partial u}{\partial x} + \frac{\partial v}{\partial y} = 0, \quad u\frac{\partial u}{\partial x} + v\frac{\partial u}{\partial y} = -\frac{\partial p}{\partial x} + \nabla^2 u, \tag{2.5a,b}$$

$$u\frac{\partial v}{\partial x} + v\frac{\partial v}{\partial y} = -\frac{\partial p}{\partial y} + \nabla^2 v + \text{Pr}^{-1}\,\theta, \quad u\frac{\partial \theta}{\partial x} + v\frac{\partial \theta}{\partial y} = \text{Pr}^{-1}\nabla^2\theta, \tag{2.5c,d}$$

where (u, v) are the velocity components in the (x, y) directions, respectively, scaled with $U_v{}^* = \nu^*/h^*$ as the velocity scale, p stands for the pressure scaled with $\rho^* U_v^{*2}$ as the pressure scale, and $\text{Pr} = \nu^*/\kappa^*$ is the Prandtl number. These equations are subject to boundary conditions (2.4) combined with

$$u(-1) = 0, \quad u(1) = \text{Re}, \tag{2.6a}$$

$$v(-1) = 0, \quad v(1) = 0, \tag{2.6b}$$

where $U_{\text{top}}^*/U_v{}^* = \text{Re}$. As the flow is driven by the movement of the upper plate, the mean pressure gradient is eliminated through imposition of constraint of the form

$$\left.\frac{\partial p}{\partial x}\right|_{\text{mean}} = 0. \tag{2.7}$$

Heating alters the flow, leading to changes of the shear stress acting on the upper plate, $\Delta\tau^* = \tau^* - \tau_0^*$, which, when scaled with $U_v^*\mu^*/h^*$, can be expressed as

$$\Delta\tau = -\left.\frac{du}{dy}\right|_{y=1} + \frac{1}{2}\text{Re} \tag{2.8}$$

and results in the change in the overall driving force, $\Delta F^* = F_0^* - F^*$, which, when scaled with $\rho^* U_v^{*2}$, can be evaluated using the following relation:

$$\Delta F = F_0 - F = \text{Re}\left(\frac{1}{2} - \text{Re}^{-1}\lambda^{-1}\int_0^\lambda \left.\frac{du}{dy}\right|_{y=1} dx\right). \tag{2.9}$$

The pressure is constant under isothermal conditions but becomes periodic when heating is added resulting in an additional lifting force G^* acting on the upper plate. This force scaled with $\rho^* U_v^{*2}$ can be evaluated according to the following formula:

$$G = \lambda^{-1}\int_0^\lambda p|_{y=1} dx. \tag{2.10}$$

The heating affects also the flow rate whose change, $\Delta Q^* = Q^* - Q_0^*$, scaled with $U_v{}^*$ is described by the following formula:

$$\Delta Q = \text{Re}\left\{\text{Re}^{-1}\left[\int_{-1}^{1} u(x, y)\, dy\right]\right|_{\text{mean}} - 1\Bigg\}. \tag{2.11}$$

The amount of heat transferred between the plates can be viewed as an energy cost associated with the flow-re-arrangements and can be quantified in terms of the mean Nusselt number defined as

$$\mathrm{Nu}_{av} = \lambda^{-1} \int_0^{\lambda} \left. \frac{\partial \theta}{\partial y} \right|_{y=1} dx. \tag{2.12}$$

System (2.5)–(2.7) was expressed in terms of the stream function defined in the usual manner, $u = \frac{\partial \psi}{\partial y}$, $v = -\frac{\partial \psi}{\partial x}$, leading to the field equations of the following form:

$$\nabla^4 \psi - \mathrm{Pr}^{-1} \frac{\partial \theta}{\partial x} = N_{VV}, \quad \nabla^2 \theta = \mathrm{Pr}\, N_{V\theta}, \tag{2.13}$$

where $N_{VV} = \frac{\partial}{\partial y}(\frac{\partial}{\partial x}\widehat{uu} + \frac{\partial}{\partial y}\widehat{uv}) - \frac{\partial}{\partial x}(\frac{\partial}{\partial x}\widehat{uv} + \frac{\partial}{\partial y}\widehat{vv})$, $N_{V\theta} = \frac{\partial}{\partial x}\widehat{u\theta} + \Gamma \frac{\partial}{\partial \hat{y}}\widehat{v\theta}$ and the hat identifies product of two unknowns. The x dependence of the unknowns was captured by expressing them as well as all products as Fourier expansions based on the heating wave number α:

$$q(x, y) = \sum_{n=-\infty}^{n=+\infty} q^{(n)}(y) e^{in\alpha x}, \tag{2.14}$$

where q stands for any of the following quantities: $\psi, \theta, p,\ u,\ v, \widehat{uu},\ \widehat{uv}, \widehat{vv}, \widehat{u\theta}, \widehat{v\theta}$. These expansions were substituted into (2.13) and the Fourier modes were separated leading to a system of nonlinear ordinary differential equations for the modal functions. This system was solved using two distinct methods. The first method used the variable-step-size finite-difference approximation [17], and the second method used the Chebyshev collocation method [19]. The numerical parameters selected for this study guaranteed at least six digits agreement between results produced by both methods. The results were also checked by comparing them with analytic solutions for small and large α limits presented in Appendices A and B. The pressure was determined using 2.5(b) and 2.5(c) from the known velocity and temperature fields using (2.5b) and 2.5(c). It was assumed that pressure was zero under isothermal conditions and, thus, its nonisothermal modifications were normalized by bringing their mean value to zero.

III. DESCRIPTION OF SYSTEM DYNAMICS

A. Plates with equal mean temperatures

Identical mean temperatures of both plates correspond to $\mathrm{Ra}_{\mathrm{uni}} = 0$. When the upper plate is stationary ($\mathrm{Re} = 0$), a purely periodic heating results in the formation of convective counter-rotating rolls with the fluid moving upwards above the hot spots and downwards above the cold spots, as illustrated in Fig. 2(a), and its temperature rising above the mean in most of the fluid volume. Slow movement of the upper plate ($\mathrm{Re} = 1$) results in a competition between the plate-driven and the buoyancy-driven motions. The flow topology is simple in the zones with the clockwise-rotating rolls as the roll movement is kinematically consistent with the plate movement, resulting in the formation of a single stream of fluid moving in the positive x-direction located in the immediate vicinity of the moving plate. A complex flow topology forms in the zones with the counterclockwise-rotating rolls as the fluid stream splits into two branches, one flowing above the rolls and one flowing beneath them. The upper branch is dominated by the plate effect, and the lower branch is dominated by the roll effect [see Fig. 2(b)]. Most of the fluid remains trapped in the rolls, i.e., either in the clockwise rolls attached to the lower plate or in the counterclockwise rolls bounded by the two branches of the stream moving to the right. The complexity of this topology near the upper plate is illustrated in Fig. 3. A further increase of the plate velocity ($\mathrm{Re} = 5$) results in the dominance of the plate-driven movement with most of the fluid moving to the right, the elimination of the counterclockwise rolls and the reduction of the size of the clockwise rolls [see Fig. 2(c)] but with the buoyancy effects still providing a significant contribution to the overall flow dynamics. A further increase of Re results in the eventual elimination of the rolls [see topology for $\mathrm{Re} = 50$ in Fig. 2(d)]. The sequence of plots

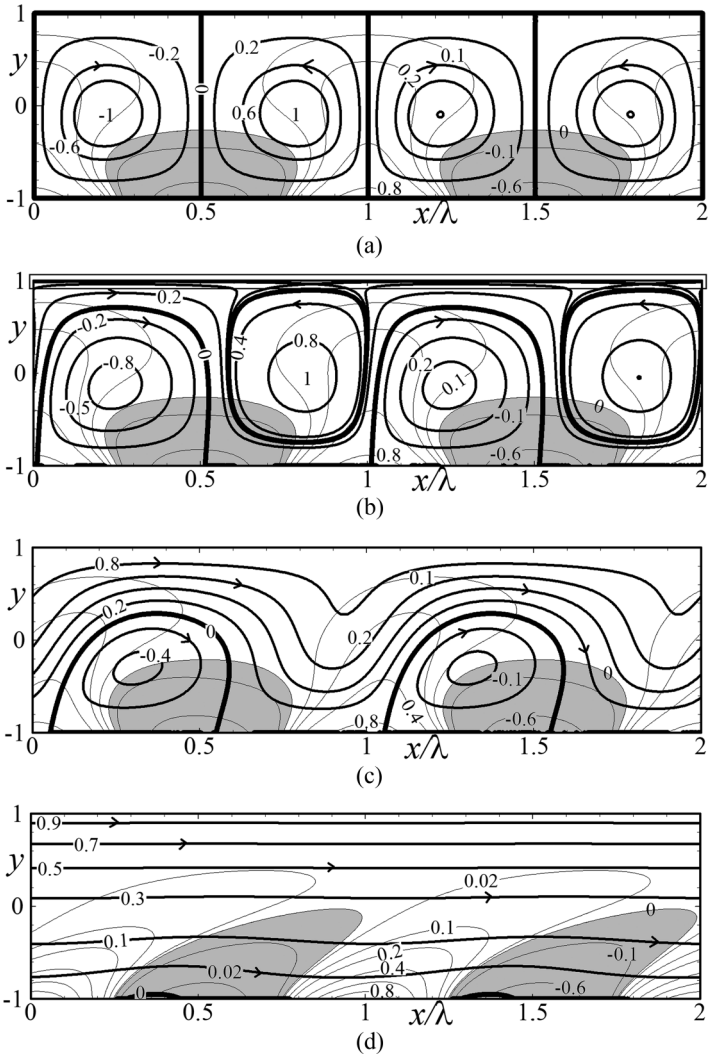

FIG. 2. The flow and temperature fields for $\mathrm{Ra}_P = 1000$, $\mathrm{Pr} = 0.71$, $\mathrm{Ra}_{\mathrm{uni}} = 0$, $\alpha = 2$ and (a) $\mathrm{Re} = 0$, (b) $\mathrm{Re} = 1$, (c) $\mathrm{Re} = 5$, (d) $\mathrm{Re} = 50$. Thick lines identify streamlines, thin lines identify isotherms, gray shadings identify zones of cold fluid. Thick streamlines mark borders of bubbles trapping the fluid. Enlargement of box shown in panel (b) is displayed in Fig. 3. Flow conditions used in these plots are marked in Fig. 10 using squares.

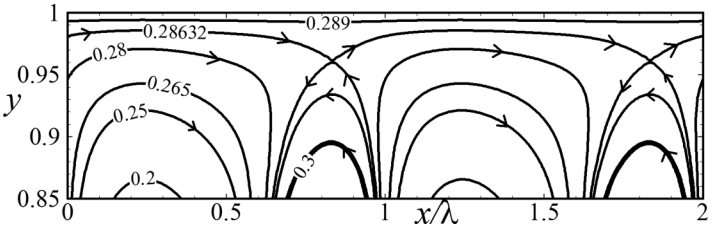

FIG. 3. Enlargement of the box shown in Fig. 2(b). The streamline emanating from the in-flow stagnation points corresponds to $\psi = 0.286322$.

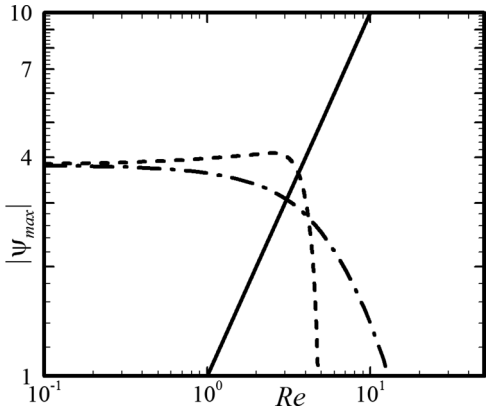

FIG. 4. Variations of the local $|\psi_{\max}|$ associated with the upper plate (solid line), the clockwise rolls (dashed line), and the counterclockwise rolls (dashed-dotted line) as functions of Re for $\alpha = 2$, $\mathrm{Ra}_P = 1000$, $\mathrm{Pr} = 0.71$, $\mathrm{Ra}_{\mathrm{uni}} = 0$.

displayed in Fig. 2 illustrates the process of formation of both the flow and thermal boundary layers near the lower plate as Re increases. Variations of the local maxima of the stream function associated with the upper plate movement and with both types of rolls as functions of Re (Fig. 4) demonstrate that the dominance of the upper plate begins for $\mathrm{Re} > 4$ and, for such conditions, the movement of the clockwise rolls results from both the buoyancy effects as well as the plate-induced pull.

In an isothermal system, the force F_0 given by Eq. (2.1) is required to maintain the motion of the plate. This force is created by friction which is responsible for fluid being dragged by the plate. For nonisothermal systems, results displayed in Fig. 2 suggest that the buoyancy-driven roll rotation assists with the fluid movement likely reducing the need for the external driving force F but this prediction needs to be confirmed through solution of (2.5)–(2.7). The shear stress acting on the plate varies periodically in x with its amplitude significantly exceeding the isothermal stress (see Fig. 5). Its mean value decreases below the isothermal stress and may even change direction. In the latter case, the convection-generated stresses are large enough so that the external force must change direction

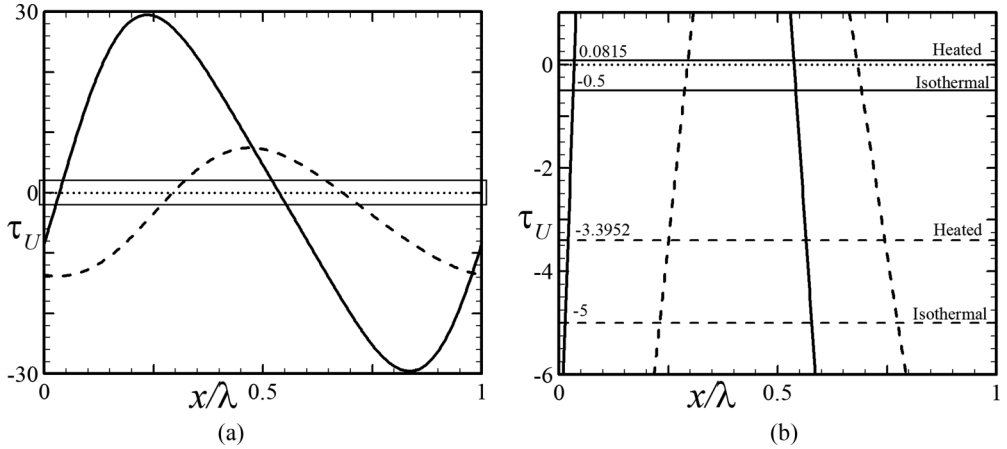

FIG. 5. Distribution of the shear stress τ_U acting on the upper plate for $\alpha = 2$, $\mathrm{Ra}_P = 1000$, $\mathrm{Pr} = 0.71$, $\mathrm{Ra}_{\mathrm{uni}} = 0$ at $\mathrm{Re} = 1$ (solid line) and $\mathrm{Re} = 10$ (dashed line). Enlargement of the box shown in panel (a) is displayed in panel (b) including shear mean values.

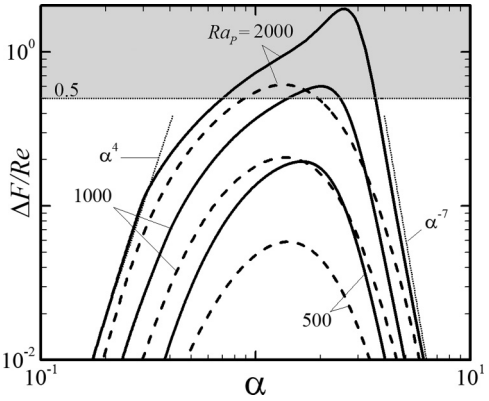

FIG. 6. Variations of $\Delta F/\mathrm{Re}$ as a function of α for $\mathrm{Pr} = 0.71$, $\mathrm{Ra_{uni}} = 0$, $\mathrm{Re} = 1$ (solid lines) and $\mathrm{Re} = 10$ (dashed lines). Thin dotted lines identify asymptotes. The shaded area identifies conditions where the driving force must change direction and becomes a braking force.

and act as a brake to prevent plate acceleration and to maintain its prescribed velocity. The positive difference $\Delta F = F_0 - F$ [see Eq. (2.9)] identifies conditions leading to the reduction of the driving force and $\Delta F/\mathrm{Re} > 0.5$ identifies conditions when the driving force must change direction, i.e., its role changes from driving the plate movement to opposing its movement.

The results presented in Fig. 6 demonstrate that all heating wave numbers lead to a decrease of the driving force with the magnitude of this reduction being a strong function of α. The largest reduction occurs for $\alpha \approx 1$–2 with its magnitude decreasing proportionally to α^4 if an excessively small α is used. This reduction is also proportional to $\mathrm{Re\,Pr^2 Ra_p^2}$ (see Appendix A for details). The flow and temperature fields (not shown) are qualitatively similar to those displayed in Fig. 2. The use of an excessively large α also results in a reduction of ΔF but at a much higher rate, proportionally to α^{-7}. This reduction is also proportional to $\mathrm{Re\,Pr^{-2} Ra_p^2}$ (see Appendix B). Plots of the temperature fields displayed in Fig. 7 demonstrate that a sufficient increase in α leads to the formation of a boundary layer close to the lower plate containing convective effects and a conductive layer with a very simple flow topology above it (see Appendix B for further details). The qualitatively different dependence on Pr for small and large α shows a relatively stronger role of conduction for large α's and a relatively stronger role of convection for small α's.

Heating affects the volume of fluid driven to the right by the plate motion. The flow rate generally increases with Ra_p, as illustrated in Fig. 8, as the buoyancy force assists the motion of the plate. The maximum increase occurs for the same α's as those which produce the largest force reduction. There are special cases, however, where a combination of a sufficiently large Ra_p with a proper range of small α's results in a decrease in the flow rate. This is caused by the formation of various in-flow separation bubbles which block the fluid motion in the positive x direction as illustrated in Fig. 9. Regardless, the flow rate always increases if α is sufficiently small as demonstrated in Appendix A.

The heating-induced motion modifies the pressure field as illustrated in Fig. 10. The fluid is driven upwards above the hot spots by the buoyancy force. It turns sideways as it approaches the upper plate with the local pressure maxima at the upper plate responsible for the turn. It is subsequently driven downwards above the cold spots by the negative buoyancy force with the local pressure maxima forming at the lower plate to force the fluid to turn sideways. The resulting pressure distributions at the plates have large-amplitude x-periodic variations (see Fig. 11) and generate net forces as well as moments, with the heating-induced lifting force at the upper plate G being of special interest. Variations of this force as a function of α illustrated in Fig. 12(a) demonstrate that G is largest for approximately the same conditions which lead to the largest reduction of the driving force. The evaluation of bending moments requires determination of the x-location x_{ref} where the pressure is

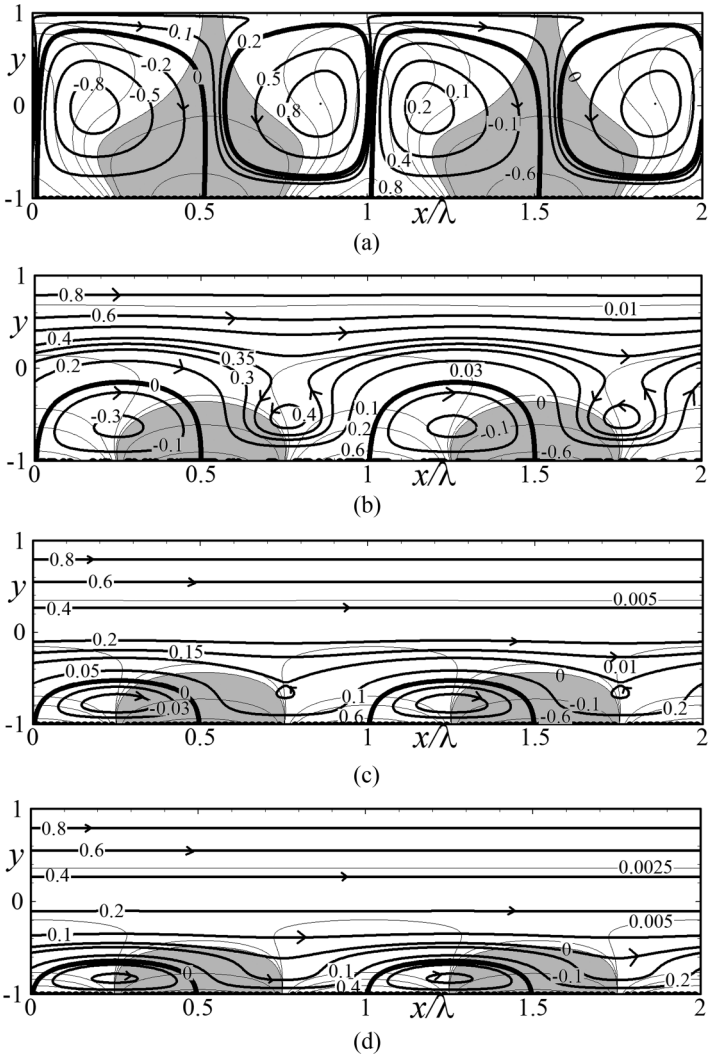

FIG. 7. The flow and temperature fields for $\mathrm{Ra}_P = 1000$, $\mathrm{Pr} = 0.71$, $\mathrm{Ra}_{\mathrm{uni}} = 0$, $\mathrm{Re} = 1$ and $\alpha = 1$ (a), $\alpha = 5$ (b), $\alpha = 8$ (c), $\alpha = 10$ (d). Thick lines identify streamlines, thin lines identify isotherms, gray shadings identify zones of cold fluid. Thick streamlines mark borders of various bubbles trapping the fluid.

equal to its mean value (see Fig. 11). The bending moment around this point is defined as

$$M = \int_{x_{\min}}^{x_{\max}} (p - p_{\mathrm{ave}})(x_{\mathrm{ref}} - x)dx, \tag{3.1}$$

where $x_{\min} = x_{\mathrm{ref}} + (x_1 - x_{\mathrm{ref}})/2$ is the location of the minimum pressure and $x_{\max} = x_{\mathrm{ref}} - (x_{\mathrm{ref}} + 1 - x_1)/2$ is the location of the maximum pressure, and the x distances are measured using fraction of the wavelength. An opposite moment acts around point x_1 (see Fig. 11), i.e., there are two moments per wavelength. The magnitude of M decreases rather rapidly for large α's [see Fig. 12(b)] due to the reduction of both the amplitude of the pressure variations as well as the plate length contributing to a single moment, while their number per unit plate length increases. Such moments are unlikely to create any structural problems. Suprisingly, M increases for small α's [see Fig. 12(b)]

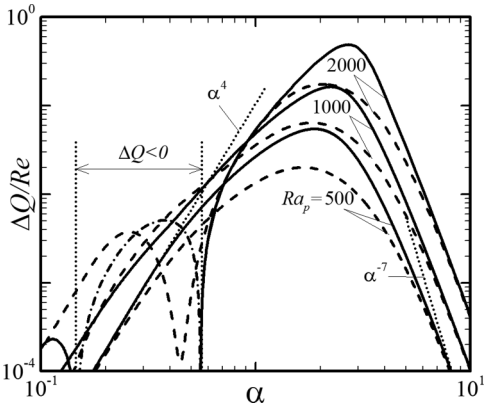

FIG. 8. Variations of change of the flow rate driven by movement of the upper plate ΔQ/Re as a function of α for Pr = 0.71, $\mathrm{Ra_{uni}} = 0$, Re = 1 (solid lines) and Re = 10 (dashed lines). Thin dotted lines identify asymptotes. Dashed-dotted line identifies the negative values of ΔQ for $\mathrm{Ra}_p = 2000$, Re = 1.

in spite of a significant reduction of the intensity of convection, and this effect is associated with an increase of the plate length reponsible for the creation of a single moment.

The force-reducing effect is a strong function of Re [see Fig. 13(a)]. The magnitude of ΔF increases proportionally to Re for small Re's, reaches a maximum at Re $\sim$ 5–6 and then decreases at a rate proportional to Re^{-2}. The flow topologies displayed in Fig. 2 show that the elimination of ΔF is associated with the reduction of convection bubbles and confinement of convection effects to a thin boundary layer near the lower plate. Variations of the flow rate follow a similar pattern [see Fig. 13(b)]: ΔQ increases at first proportionally to Re, reaches a maximum at Re $\sim$ 5–6 and then decreases at a rate proportional to Re^{-2}.

ΔF is a stronger function of Ra_p than of Re as it increases proportionally to Ra_p^2 [see Fig. 14(a)]. A saturation develops for large enough Ra_p slowing down this growth. The saturation starts at a smaller Ra_p when Re is smaller. Flow topologies displayed in Fig. 15 show expansion of the rolls and reduction of the size of the stream tube with an increase in Ra_p. The amount of fluid driven by the plate increases with Ra_p but the development of complex flow topologies (not shown) reduces this flow for a range of small α's [see Fig. 14(b)].

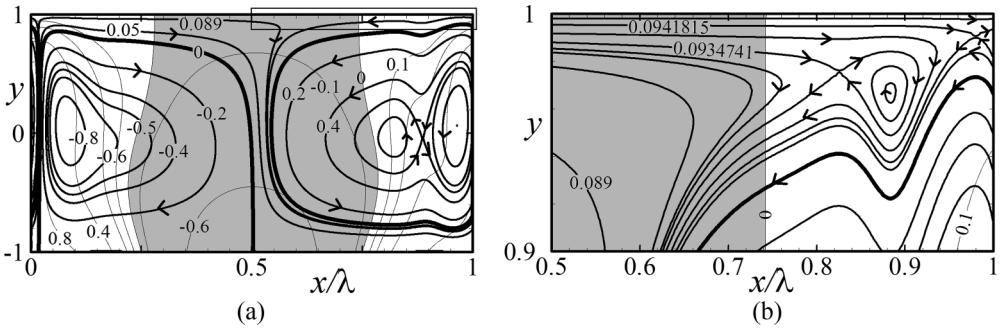

FIG. 9. The flow and temperature fields for $\mathrm{Ra}_p = 2000$, Pr = 0.71, $\mathrm{Ra_{uni}} = 0$, Re = 1, $\alpha = 0.25$. Enlargement of box in Fig. 6(a) is displayed in panel (b). Thick lines identify streamlines, thin lines identify isotherms, gray shadings identify zones of cold fluid. Thick streamlines mark borders of various bubbles trapping the fluid.

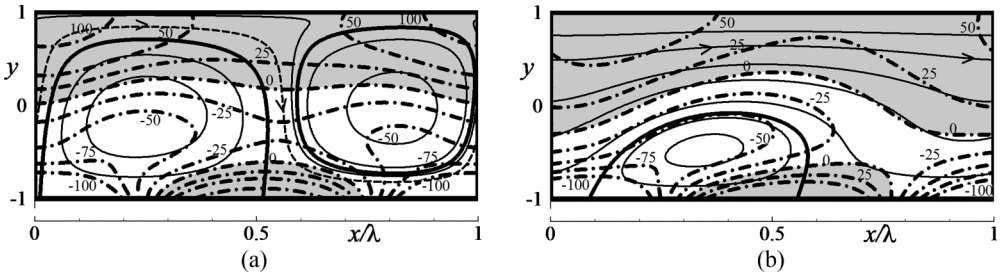

FIG. 10. Pressure fields for $\alpha = 2, \mathrm{Ra}_P = 1000, \mathrm{Pr} = 0.71, \mathrm{Re} = 1$ (a) and $\mathrm{Re} = 10$ (b). Dotted and dashed-dotted lines identify the positive and negative values, respectively. Thick solid lines illustrate streamlines. Shaded areas correspond to positive pressure.

Analyzing (2.9) shows that the external force required to drive the upper plate decreases to zero when $\Delta F = \mathrm{Re}/2$. Such conditions can be easily achieved and correspond to the gray shading in Fig. 6. When $\Delta F > \mathrm{Re}/2$, the heating-induced effects are strong enough so that the external force must change direction and act as a brake to prevent the plate from accelerating. This shows that the system becomes metastable when exposed to a periodic heating. Consider a stationary upper plate without any external forces acting on it and apply heating to the lower plate. The convection-induced forces increase with Ra_p [see Fig. 14(a)] but the system remains at rest due to its periodicity and x symmetry. The addition of any disturbance which breaks the symmetry will not generate plate motion if the heating is too weak; an external force is required to support such motion and heating is too weak to generate it. For strong enough heating, disturbances will generate plate motion as the buoyancy forces can overcome friction. As the plate accelerates (Re increases), the buoyancy forces decrease [see Fig. 13(a)] until a state of equilibrium is reached where the increased friction balances the decreased driving force. The upper plate may move in either horizontal direction depending on the form of the initial disturbance. This mechanism can be used to move a free-floating body by simply heating one of the plates.

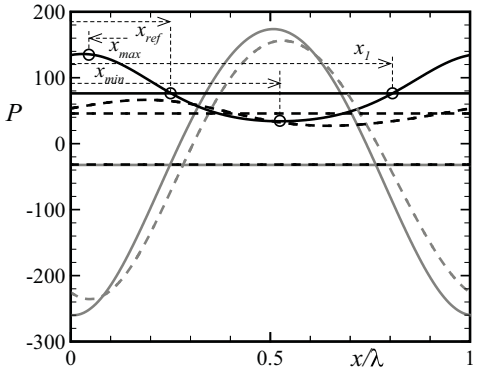

FIG. 11. Distributions of the pressure at the upper (black lines) and lower (gray lines) plates for $\alpha = 2$, $\mathrm{Ra}_P = 1000, \mathrm{Pr} = 0.71, \mathrm{Re} = 1$(solid lines) and $\mathrm{Re} = 10$ (dashed lines). The average values of pressure at the lower wall overlap within the plotting accuracy as they are -32.2, -31.7 for $\mathrm{Re} = 1$, 10, respectively. The characteristic points used in the evaluation of moments at the upper plate are marked with thin dotted lines using $\mathrm{Re} = 1$ as an example.

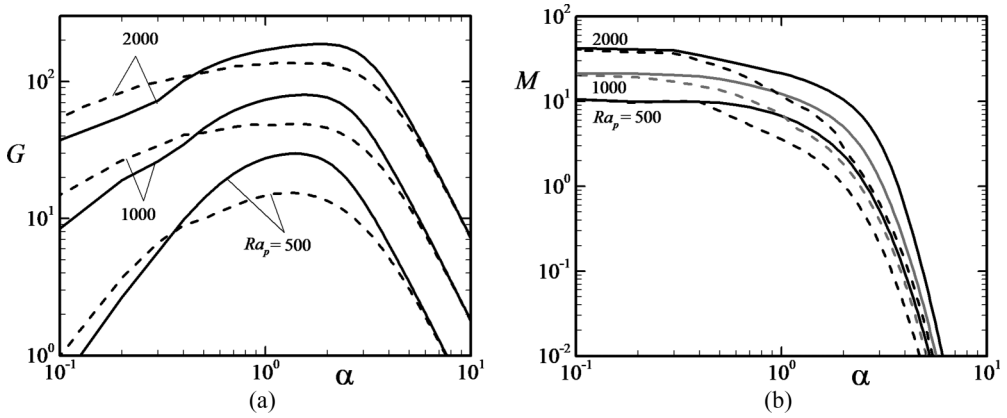

FIG. 12. Variations of the lifting force G (a) and the moment M (b) as functions of α for Pr $= 0.71$, $Ra_{\text{uni}} = 0$, Re $= 1$ (solid lines) and Re $= 10$ (dashed lines).

B. Plates with different mean temperatures

As it is unlikely that the mean temperatures of both plates can be kept equal, it is of interest to determine how their difference may affect the system response. This difference is expressed in the analysis as the uniform Rayleigh number Ra_{uni} whose positive (negative) values correspond to the lower plate being hotter (cooler). The results displayed in Fig. 16 demonstrate that the uniform heating increases ΔF while cooling decreases it, and the change is approximately linear with Ra_{uni}. The type of variations as a function of α remains nearly identical for larger Re's (see Re $= 10$ in Fig. 16) for all Ra_{uni}'s considered with an upward shift resulting from the increase of Ra_{uni}, and with the most effective α nearly unchanged. A shift from $\text{Ra}_{\text{uni}} = -150$ to $\text{Ra}_{\text{uni}} = 150$ increases ΔF by a factor of $\sim$20 when Re $= 10$, but this is not sufficient to change the direction of the driving force. In the case of smaller Re's (Re $= 1$ in Fig. 16), the most effective α shifts from $\alpha = 1.6$ to $\alpha = 2.5$, and ΔF approximately quadruples when Ra_{uni} changes in the same range, and this is sufficient to

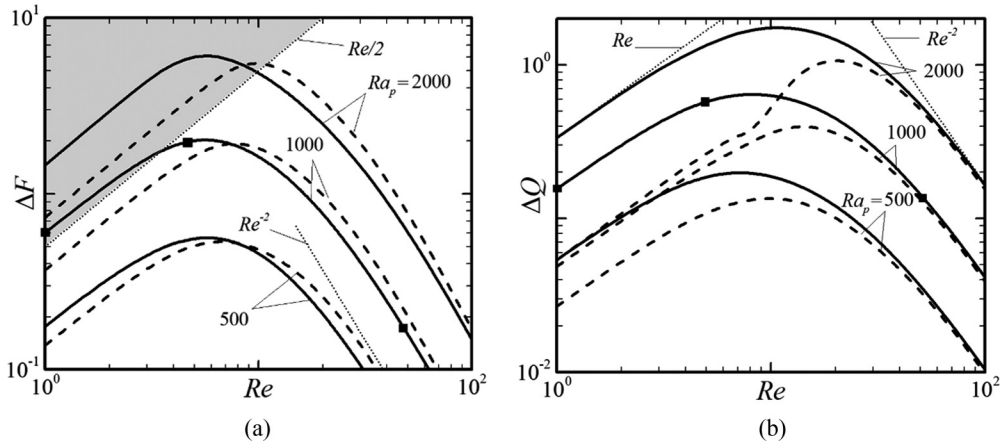

FIG. 13. Variations of ΔF (a) and ΔQ (b) as functions of Re for Pr $= 0.71$, $\text{Ra}_{\text{uni}} = 0$, $\alpha = 2$ (solid lines) and $\alpha = 1$ (dashed lines). Thin dotted lines identify asymptotes. Plots of flow and temperature field for conditions identified using squares are displayed in Fig. 2. See text for other details. The shaded area in panel (a) identifies conditions where the driving force must change direction and becomes a braking force.

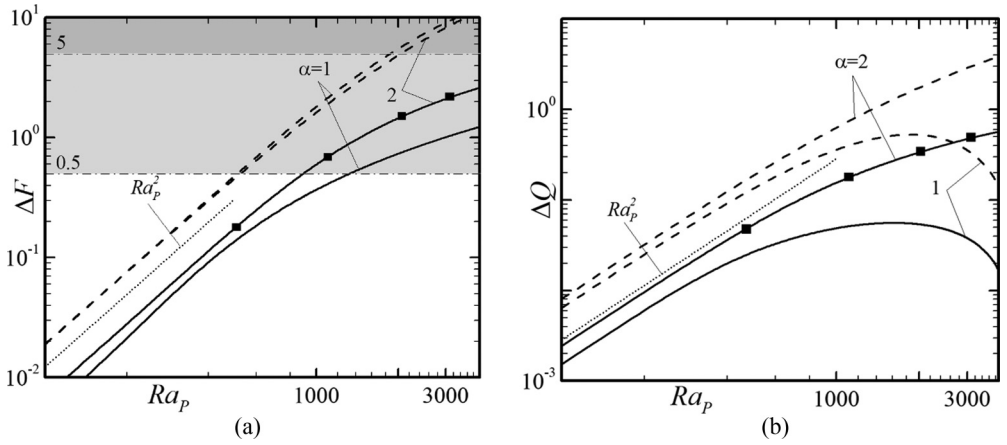

FIG. 14. Variations of ΔF (a) and ΔQ (b) as functions of Ra_p for $\mathrm{Pr} = 0.71$, $\mathrm{Ra}_{\mathrm{uni}} = 0$, $\mathrm{Re} = 1$ (solid lines) and $\mathrm{Re} = 10$ (dashed lines). Plots of flow and temperature fields for conditions identified using squares are displayed in Fig. 15. See text for other details. The shaded area identifies conditions where the driving force must change direction and becomes a braking force when $\mathrm{Re} = 1$ and the double shaded area identifies such conditions for $\mathrm{Re} = 10$.

change the direction of the driving force. Variations of the flow rate ΔQ follow the same pattern as variations of ΔF and have similar magnitudes regardless of Re (see Fig. 17).

C. Effects of the Prandtl number Pr

The Prandtl number describes transport properties with conductive effects expected to play a larger role in the small-Pr fluids. The spatial temperature variations will be stronger and less affected by convection in such fluids, leading to larger changes of ΔF. The results displayed in Fig. 18(a)

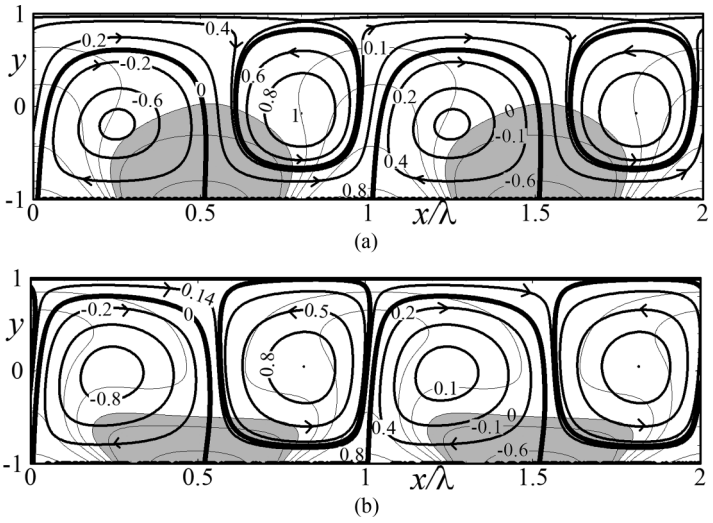

FIG. 15. The flow and temperature fields for $\mathrm{Re} = 1$, $\mathrm{Pr} = 0.71$, $\mathrm{Ra}_{\mathrm{uni}} = 0$, $\alpha = 2$ at (a) $\mathrm{Ra}_p = 500$ and (b) $\mathrm{Ra}_p = 3000$. Thick lines identify streamlines, thin lines identify isotherms, gray shadings identify zones of cold fluid. Thick streamlines mark borders of various bubbles trapping the fluid. Flow conditions used in these plots are marked in Fig. 14 using squares.

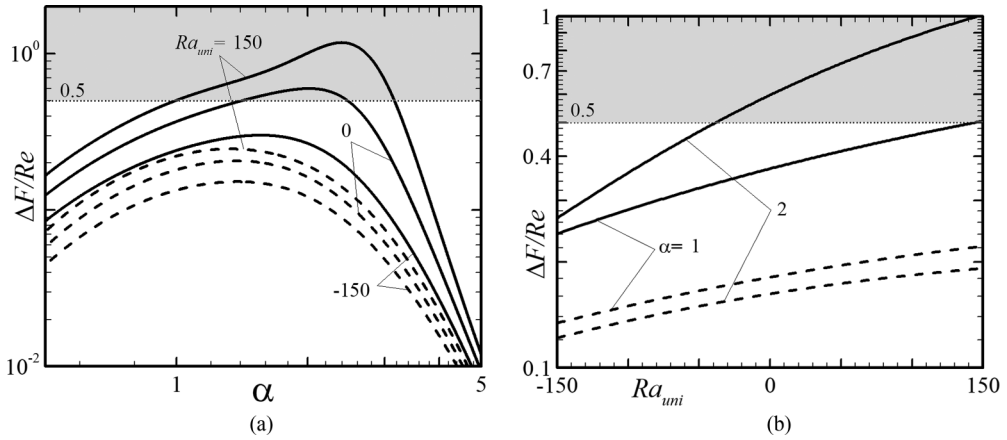

FIG. 16. Variations of $\Delta F/\mathrm{Re}$ as a function of α (a) and as a function of $\mathrm{Ra_{uni}}$ (b) for $\mathrm{Re} = 1$ (solid lines) and $\mathrm{Re} = 10$ (dashed lines), and $\mathrm{Ra}_P = 1000$, $\mathrm{Pr} = 0.71$. The shaded areas identify conditions where the driving force changes direction and becomes a braking force.

demonstrate a nearly three-orders of the magnitude increase of ΔF resulting from replacing fluids with $\mathrm{Pr} = 10$ with fluids with $\mathrm{Pr} = 0.1$, changing ΔF from being insufficient to change the direction of the driving force at large Pr's to being more than sufficient at small Pr's. The increase of the flow rate follows the same pattern as documented in Fig. 18(b). The character of the changes in ΔF and ΔQ as functions of α remains qualitatively similar for all Pr's with the relevant curves just shifted upwards for smaller Pr's as illustrated in Fig. 19.

IV. HEAT TRANSFER EFFECTS

The temperature differences between and along the plates lead to the formation of vertical and horizontal heat fluxes. The former one is of interest as the heat flow between the plates can be viewed as a potential energy cost associated with the use of heating to reduce the driving force. This heat flux can be created only by convection in the case of a purely periodic heating. Variations of the corresponding mean Nusselt number Nu_{av} displayed in Fig. 20(a) demonstrate that Nu_{av} is a strong

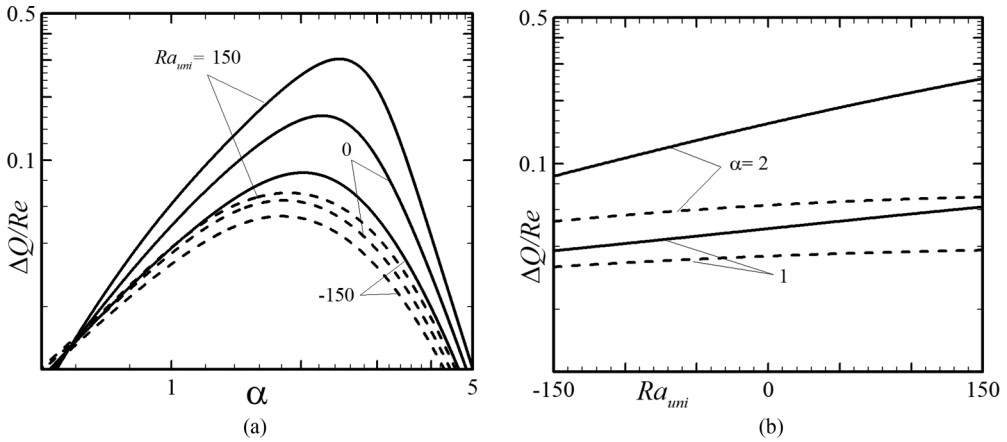

FIG. 17. Variations of $\Delta Q/\mathrm{Re}$ (a) as a function of α and as a function of $\mathrm{Ra_{uni}}$ (b) for $\mathrm{Re} = 1$ (solid lines) and $\mathrm{Re} = 10$ (dashed lines), and $\mathrm{Ra}_P = 1000$, $\mathrm{Pr} = 0.71$.

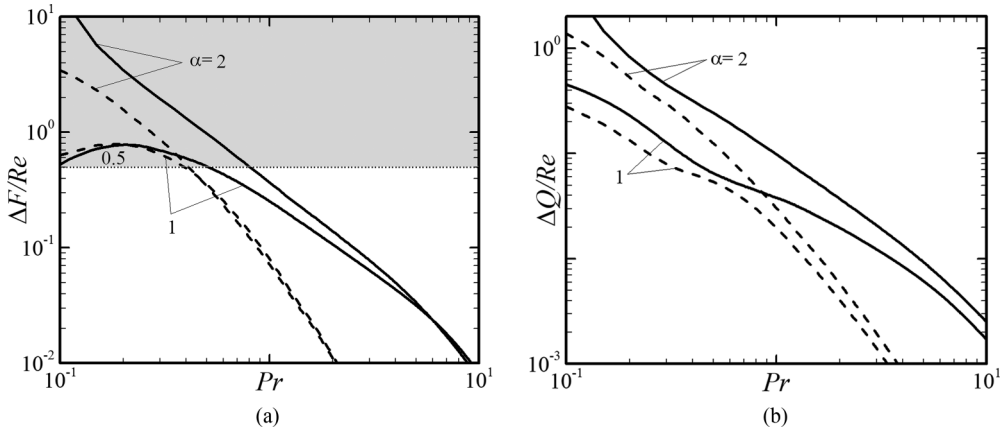

FIG. 18. Variations of (a) $\Delta F/\mathrm{Re}$ and (b) $\Delta Q/\mathrm{Re}$ as functions of Pr at Re = 1 (solid lines) and Re = 10 (dashed lines) for $\mathrm{Ra}_P = 1000$, $\mathrm{Ra}_{\mathrm{uni}} = 0$.

function of α and reaches a maximum at $\alpha \approx 0.8$–1, which is smaller than the α required to maximize ΔF. The use of an excessively small α reduces Nu_{av} at a rate proportional to α^2 (see Appendix A), which is much slower than the reduction of ΔF. The use of an excessively large α reduces Nu_{av} at a rate proportional to α^{-3} (see Appendix B), which is also much slower than the reduction of ΔF. The maximal Nu_{av} occurs at Re = 0 with an increase in Re reducing Nu_{av} [see Fig. 20(b)] through the elimination of convective effects (see Fig. 13). An increase in Ra_p results in an increase in Nu_{av} proportional to Ra_p^2, which is the same as the rate of increase of ΔF, with a very slight reduction of this growth due to saturation effects in the upper range of Ra_p's considered in this study [Fig. 20(c)]. The addition of a uniform heating component leads to a change in the heat flow due to both changes in the intensity of convection as well as due to the addition of a conductive flux. Nu_{av} increases when the lower plate is heated and decreases when it is cooled, varying in a qualitatively similar manner as a function of α for all Re's of interest with the relevant curves shifted upwards as $\mathrm{Ra}_{\mathrm{uni}}$ increases [see Fig. 21(a)]. The increase is nearly linear in the range of $\mathrm{Ra}_{\mathrm{uni}}$ of interest with the rate of change being a strong function of α [see Fig. 21(b)].

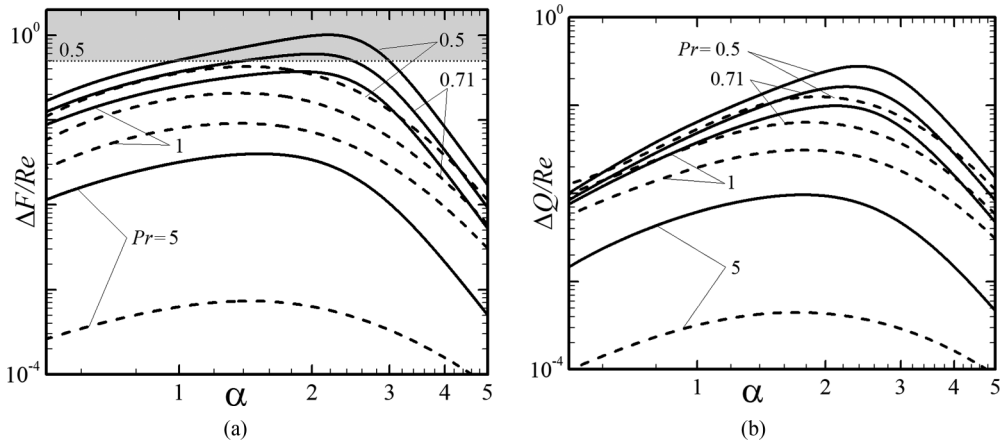

FIG. 19. Variations of (a) $\Delta F/\mathrm{Re}$ and (b) $\Delta Q/\mathrm{Re}$ as functions of α at Re = 1 (solid lines) and Re = 10 (dashed lines) for $\mathrm{Ra}_P = 1000$, $\mathrm{Ra}_{\mathrm{uni}} = 0$.

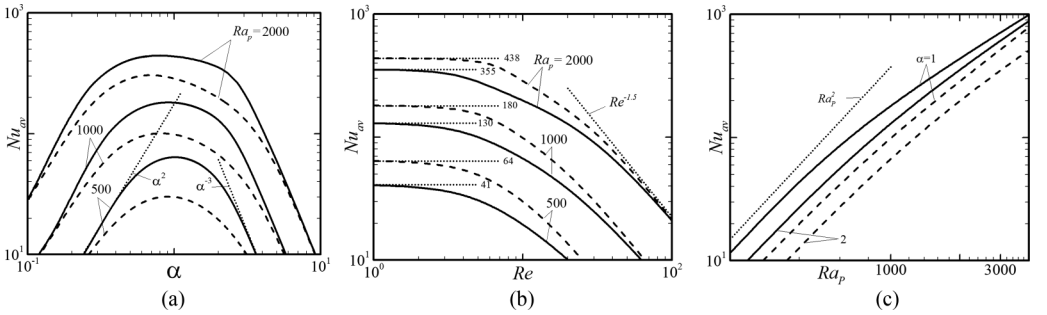

FIG. 20. Variations of Nu_{av} in panel (a) as a function of α for $\mathrm{Re} = 1$ (solid lines) and $\mathrm{Re} = 10$ (dashed lines), in panel (b) as a function of Re for $\alpha = 1$ (dashed lines) and $\alpha = 2$ (solid lines), and in panel (c) as a function of Ra_p for $\mathrm{Re} = 1$ (solid lines) and $\mathrm{Re} = 10$ (dashed lines), for $\mathrm{Pr} = 0.71$, $\mathrm{Ra}_{\mathrm{uni}} = 0$. Thin dotted lines identify asymptotes.

Changes in the heat flow due to a change of the type of fluid being used are illustrated in Fig. 22 for purely periodic heating. When Re is small and buoyancy-driven effects dominate, an increase in Pr reduces Nu_{av} in a qualitatively similar manner for all α's [see results for $\mathrm{Re} = 1$ in Fig. 22(a)] with an asymptote developing for small Pr [see Fig. 22(b)]. An increase in Re weakens convective effects and results in a significant reduction of Nu_{av} associated with an increase in Pr [see results in Fig. 22 for $\mathrm{Re} = 10$]. This reduction depends on α and a decrease in Pr may either increase or decrease the heat flux depending on the α being used.

V. HEATING OF THE UPPER PLATE

Similar effects can be achieved by heating the upper stationary plate and imposing motion of the lower plate. The similarity between both systems can be demonstrated by reversing the direction of gravity, $\mathrm{Ra}_p \rightarrow -\mathrm{Ra}_p$, and changing the sign of the temperature, $\theta \rightarrow -\theta$ [20]. The latter condition implies a change of the sign of the temperature imposed at the upper plate and results in a shift of the temperature field by a half-cycle in the x direction. The up-down "symmetry" between the lower and upper heating is illustrated in Fig. 23, and this leads to the conclusion that the externally imposed driving force is the same regardless of which plate is heated.

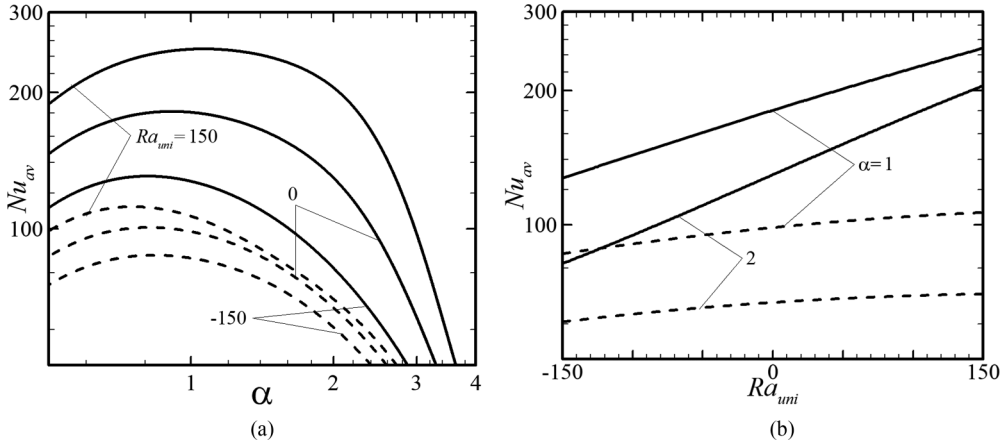

FIG. 21. Variations of Nu_{av} in panel (a) as a function of α and in panel (b) as a function of $\mathrm{Ra}_{\mathrm{uni}}$ for $\mathrm{Re} = 1$ (solid lines) and $\mathrm{Re} = 10$ (dashed lines) for $\mathrm{Ra}_p = 1000$, $\mathrm{Pr} = 0.71$.

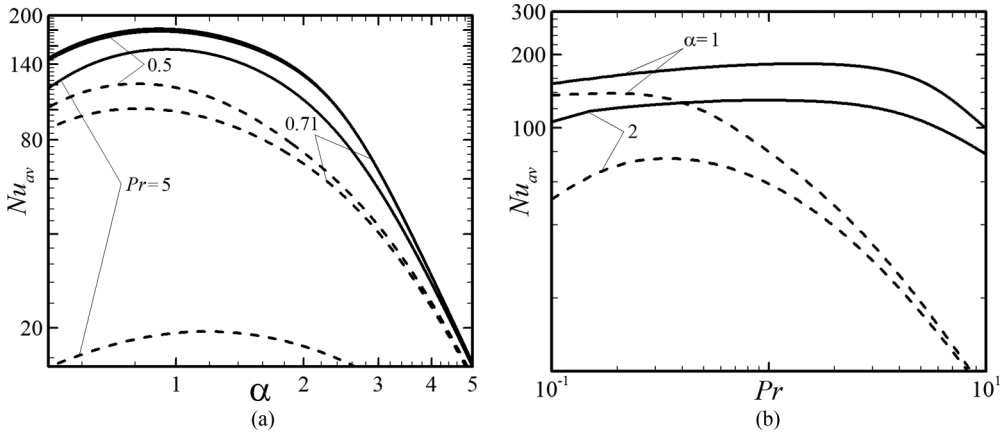

FIG. 22. Variations of Nu_{av} in panel (a) as a function of α and in panel (b) as a function of Pr for $\mathrm{Re} = 1$ (solid lines) and $\mathrm{Re} = 10$ (dashed lines) for $\mathrm{Ra}_p = 1000$, $\mathrm{Ra}_{\mathrm{uni}} = 0$.

VI. SUMMARY

An external force is required to generate a relative motion between horizontal plates with the rate of this motion expressed in terms of the Reynolds number Re. The effects of spatially distributed heating on the magnitude of this force have been analyzed. Heating resulting in the lower plate temperature varying sinusoidally in the horizontal direction, with its amplitude expressed in terms of a periodic Rayleigh number Ra_p and the spatial distribution described by the wave number α, has been considered. The analysis has been limited to $\mathrm{Ra}_p < 2000$ to avoid condition leading to a potential formation of secondary flows. The difference between the mean plates' temperatures has been expressed in terms of the uniform Rayleigh number $\mathrm{Ra}_{\mathrm{uni}}$ with positive values corresponding to a warmer lower plate. The fluid motion results from a competition between the buoyancy-driven effects and the plate-driven movement. The former has the form of counter-rotating rolls whose distribution is dictated by the heating pattern. The latter one adds a rectilinear motion which leads to the reduction and eventual elimination of the rolls if Re is large enough.

It has been shown that periodic heating always reduces the driving force, regardless of whether the heating is applied to the lower or upper plate, but the magnitude of this reduction is a strong function of the heating wave number. The largest reduction is achieved for $\alpha = 1 - 2$ with a rapid decrease of this effect when either too small or too large α's are used. An increase in $\mathrm{Ra}_{\mathrm{uni}}$ and decrease in the Prandtl number Pr magnify this effect. An increase in Re eliminates the rolls and reduces this effect, leading to its practical elimination for $\mathrm{Re} > 30$–50 depending on the heating intensity. The use of proper heating intensity and distribution results in the complete elimination of the driving force as the plate movement can be supported by the buoyancy effects only. Conditions where an external braking force needs to be used to prevent the plate from accelerating have also

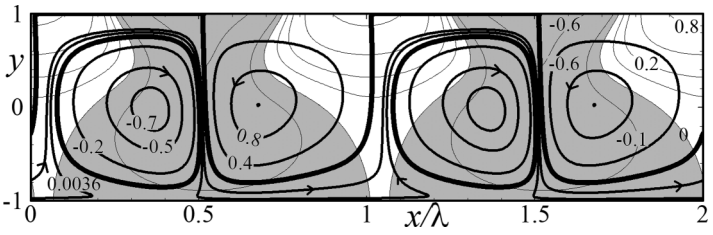

FIG. 23. The flow and temperature fields for the same conditions as in Fig. 7(a) but with the upper plate heated and the lower plate moving. Thick lines identify streamlines, thin lines identify isotherms, gray shadings identify zones of cold fluid. Thick streamlines mark borders of bubbles trapping the fluid.

been identified. It has been shown that a stationary system, which allows a free movement of one of the plates, is metastable when exposed to periodic heating as motion of the plate in any direction may result from application of an external disturbance if the heating intensity and distribution meet certain conditions; these conditions have been explicitly identified.

Conditions used in the analysis were selected to avoid formation of secondary states. These conditions were selected based on information available in the literature, however, a stability analysis should be carried out to confirm these predictions.

ACKNOWLEDGMENT

This work has been carried out with the support of NSERC of Canada.

APPENDIX A: LONG-WAVELENGTH HEATING ($\alpha \to 0$)

Introduction of a slow scale $X = \alpha\, x$, representation of the unknowns as power series of α:

$$[u(X,y), v(X,y), \theta(X,y)] = \sum_{n=0}^{n=4} \alpha^n [U_n(X,y), V_n(X,y), \Theta_n(X,y)] + O(\alpha^5), \tag{A1a}$$

$$p(X,y) = \sum_{n=-1}^{n=3} \alpha^n P_n(X,y) + O(\alpha^5), \tag{A1b}$$

$$\Delta F = \sum_{n=0}^{4} \Delta F_n\, \alpha^n, \quad \Delta Q = \sum_{n=0}^{4} \Delta Q_n\, \alpha^n, \quad \mathrm{Nu}_{av} = \sum_{n=0}^{4} \mathrm{Nu}_{av,n}\, \alpha^n, \tag{A2}$$

substitution of (A1) into the field equations and extraction of the leading-order terms result in the following system:

$$\frac{\partial^2 U_0}{\partial y^2} - V_0 \frac{\partial U_0}{\partial y} = \frac{\partial P_{-1}}{\partial X}, \quad \frac{\partial V_0}{\partial y} = 0, \quad \frac{\partial P_{-1}}{\partial y} = 0, \quad \frac{\partial^2 \Theta_0}{\partial y^2} = \mathrm{Pr} V_0 \frac{\partial \Theta_0}{\partial y}, \tag{A3a–d}$$

$$U_0(X,1) = \mathrm{Re}, \quad U_0(X,-1) = 0, \quad V_0(X,\pm 1) = 0, \tag{A3e–g}$$

$$\Theta_0(X,-1) = \mathrm{Ra}_{\mathrm{uni}} + 0.5\mathrm{Ra}_p \cos X, \quad \Theta_0(X,1) = 0, \quad \left.\frac{\partial P_{-1}}{\partial X}\right|_{\mathrm{mean}} = 0, \tag{A3h–j}$$

whose solution has the form of

$$U_0 = \mathrm{Re}(1+y)/2, \quad V_0 = 0, \quad P_{-1} = 0, \quad \Theta_0 = (1-y)(2\mathrm{Ra}_{\mathrm{uni}} + \mathrm{Ra}_p \cos X)/4, \tag{A4a–d}$$

$$\Delta F_0 = 0, \quad \Delta Q_0 = 0, \quad \mathrm{Nu}_{av,0} = \mathrm{Ra}_{\mathrm{uni}}/2. \tag{A4e–g}$$

The next-order system can be written as

$$\frac{\partial^2 U_1}{\partial y^2} = \frac{\partial P_0}{\partial X}, \quad \frac{\partial V_1}{\partial y} = -\frac{\partial U_0}{\partial X}, \quad \frac{\partial P_0}{\partial y} = \mathrm{Pr}^{-1}\Theta_0, \quad \frac{\partial^2 \Theta_1}{\partial y^2} = \mathrm{Pr} U_0 \frac{\partial \Theta_0}{\partial X} + \mathrm{Pr} V_1 \frac{\partial \Theta_0}{\partial y}, \tag{A5a–d}$$

$$U_1(X,\pm 1) = 0, \quad V_1(X,\pm 1) = 0, \quad \Theta_1(X,\pm 1) = 0, \quad \left.\frac{\partial P_0}{\partial X}\right|_{\mathrm{mean}} = 0 \tag{A5e–h}$$

and has a solution of the form

$$U_1(X,y) = \mathrm{Pr}^{-1}\mathrm{Ra}_p\, L_{U1}(y) \sin X, \quad V_1 = 0,$$

$$P_0(X,y) = \mathrm{Pr}^{-1}\mathrm{Ra}_p\, L_{P01}(y) \cos X + \mathrm{Pr}^{-1}\mathrm{Ra}_{\mathrm{uni}} L_{P02}(y), \tag{A6a–c}$$

$$\Theta_1(X,y) = \mathrm{Pr}\,\mathrm{Re}\mathrm{Ra}_p\, L_{\Theta 1}(y) \sin X, \quad \Delta F_1 = 0, \quad \Delta Q_1 = 0, \quad \mathrm{Nu}_{av,1} = 0, \tag{A6d–g}$$

where $L_{U1} = \frac{1}{480} + \frac{y}{24} - \frac{y^2}{80} - \frac{y^3}{24} + \frac{y^4}{96}$, $L_{V2} = \frac{1}{480}(5-y)(-1+y^2)^2$, $L_{\Theta 1} = \frac{1}{96}(5-6y^2+y^4)$, $L_{P01} = \frac{1}{40} + \frac{y}{4} - \frac{y^2}{8}$, $L_{P02} = \frac{y}{2} - \frac{y^2}{4}$.

The follow-up system has the form

$$\frac{\partial^2 U_2}{\partial y^2} = \frac{\partial P_1}{\partial X} + U_0\frac{\partial U_1}{\partial X} + \frac{dU_0}{\partial y}V_2, \quad \frac{\partial V_2}{\partial y} = -\frac{\partial U_1}{\partial X},$$

$$\frac{\partial P_1}{\partial y} = \mathrm{Pr}^{-1}\Theta_1, \quad \frac{\partial^2 \Theta_2}{\partial y^2} = \mathrm{Pr}U_0\frac{\partial \Theta_1}{\partial X} - \frac{\partial^2 \Theta_0}{\partial X^2} + \mathrm{Pr}U_1\frac{\partial \Theta_0}{\partial X} + \mathrm{Pr}V_2\frac{\partial \Theta_0}{\partial y}, \quad \text{(A7a–d)}$$

$$U_2(X,\pm 1) = 0, \quad V_2(X,\pm 1) = 0, \quad \Theta_2(X,\pm 1) = 0, \quad \left.\frac{\partial P_1}{\partial X}\right|_{\mathrm{mean}} = 0, \quad \text{(A7e–h)}$$

and its solution can be represented as

$$U_2(X,y) = \mathrm{Pr}^{-1}\mathrm{Re}\,\mathrm{Ra}_p L_{U2}(y)\cos X, \quad V_2(X,y) = \mathrm{Pr}^{-1}\mathrm{Ra}_p L_{V2}(y)\cos X,$$

$$P_1 = \mathrm{Pr}^{-1}\mathrm{Re}\,\mathrm{Ra}_p L_{P1}\sin X, \quad \text{(A8a–c)}$$

$$\Theta_2(X,y) = \mathrm{Ra}_p^2\, L_{\Theta 21}(y) + \mathrm{Ra}_p[L_{\Theta 22}(y) + \mathrm{Re}^2\mathrm{Pr}^2\, L_{\Theta 23}(y) + \mathrm{Ra}_{\mathrm{uni}} L_{\Theta 24}(y)]\cos X + \mathrm{Ra}_p^2\, L_{\Theta 25}(y)\cos(2X), \quad \text{(A8d)}$$

$$\Delta F_2 = 0, \quad \Delta Q_2 = 0, \quad \mathrm{Nu}_{av,2} = \mathrm{Ra}_p^2/1400, \quad \text{(A8e–g)}$$

where

$$L_{U2} = \tfrac{1}{100\,800}(-1+y^2)[3 + (234 + 775\,\mathrm{Pr})y - 4(29 + 25\,\mathrm{Pr})y^3 - 35y^4 + 5(2+\mathrm{Pr})y^5],$$

$$L_{V3} = \tfrac{1}{806\,400}(-1+y^2)^2[5\,\mathrm{Pr}(297 - 26y^2 + y^4) + 2(197 - 12y - 74y^2 - 20y^3 + 5y^4)],$$

$$L_{P1} = \tfrac{1}{16\,800}[-104 + 35\,\mathrm{Pr}\, y(-5+y^2)^2],$$

$$L_{\Theta 21} = 3\mathrm{C}_1(-35 - 79y + 70y^2 + 26y^3 - 35y^4 + 5y^5),$$

$$L_{\Theta 22} = 5\mathrm{C}_1[-1680(-3+y)],$$

$$L_{\Theta 23} = \mathrm{C}_1(427 + 117y - 98y^2 - 58y^3 + 7y^4 + 5y^5),$$

$$L_{\Theta 24} = -2\mathrm{C}_1(-385 + 19y + 140y^2 - 16y^3 - 35y^4 + 5y^5),$$

$$L_{\Theta 25} = \mathrm{C}_1(140 - 128y + 35y^2 + 47y^3 - 35y^4 + 5y^5),$$

$$C_1 = \tfrac{1}{403\,200}(1-y^2).$$

The reader may note the appearance of a heat flux directed towards the upper plate. The next-order system has the form

$$\frac{\partial^2 U_3}{\partial y^2} = \frac{\partial P_2}{\partial X} + U_0\frac{\partial U_2}{\partial X} + \frac{dU_0}{\partial y}V_3 + U_1\frac{\partial U_1}{\partial X} + V_2\frac{\partial U_1}{\partial y} - \frac{\partial^2 U_1}{\partial X^2}, \quad \frac{\partial V_3}{\partial y} = -\frac{\partial U_2}{\partial X}, \quad \text{(A9a,b)}$$

$$\frac{\partial P_2}{\partial y} = \frac{\partial^2 V_2}{\partial y^2} + Pr^{-1}\Theta_2,$$

$$\frac{\partial^2 \Theta_3}{\partial y^2} = \mathrm{Pr}U_0\frac{\partial \Theta_2}{\partial X} - \frac{\partial^2 \Theta_1}{\partial X^2} + \mathrm{Pr}\left[U_1\frac{\partial \Theta_1}{\partial X} + V_2\frac{\partial \Theta_1}{\partial y} + U_2\frac{\partial \Theta_0}{\partial X} + V_3\frac{\partial \Theta_0}{\partial y}\right], \quad \text{(A9c,d)}$$

$$U_3(X,\pm 1) = 0, \quad V_3(X,\pm 1) = 0, \quad \Theta_3(X,\pm 1) = 0, \quad \left.\frac{\partial P_2}{\partial X}\right|_{\mathrm{mean}} = 0, \quad \text{(A9e–h)}$$

and its solution can be written as

$$U_3(X,y) = \mathrm{Pr}^{-1}\mathrm{Ra}_p[L_{U31}(y) + \mathrm{Re}^2\ L_{U32}(y) + \mathrm{Ra}_{\mathrm{uni}}L_{U33}(y)]\sin X + \mathrm{Pr}^{-1}\mathrm{Ra}_p^2\ [L_{U34}(y) + \ \mathrm{Pr}^{-1}L_{U35}(y)]\sin(2X), \tag{A10a}$$

$$V_3(X,y) = \mathrm{Pr}^{-1}\mathrm{Re}\ \mathrm{Ra}_p L_{V3}(y)\sin X, \tag{A10b}$$

$$P_2(X,y) = \mathrm{Pr}^{-1}\mathrm{Ra}_p[L_{P21}(y) + \mathrm{Re}^2\ L_{P22}(y) + \mathrm{Ra}_{\mathrm{uni}}L_{P23}(y)]\cos X + \mathrm{Pr}^{-1}\mathrm{Ra}_p^2\ [L_{P24}(y) + \mathrm{Pr}^{-1}L_{P25}(y)]\cos(2X), \tag{A10c}$$

$$\Theta_3(X,y) = \mathrm{Re}\ \mathrm{Ra}_p[\mathrm{Pr}L_{\Theta31}(y) + \mathrm{Re}^2\mathrm{Pr}^3\ L_{\Theta32}(y) + \mathrm{Ra}_{\mathrm{uni}}L_{\Theta33}(y)]\sin X + \mathrm{ReRa}_p^2\ L_{\Theta34}(y)\sin(2X), \tag{A10d}$$

$$\Delta F_3 = 0, \quad \Delta Q_3 = 0, \quad \mathrm{Nu}_{av,3} = 0. \tag{A10e–g}$$

Coefficients $L_{U31}, \ldots, L_{U35}, L_{V31}, \ldots, L_{V35}, L_{P21}, \ldots, L_{P25}, L_{\Theta31}, \ldots, L_{\Theta34}$ are not given here due to excessive length. The final system of interest in this analysis has the form

$$\frac{\partial^2 U_4}{\partial y^2} = \frac{\partial P_3}{\partial X} + U_0\frac{\partial U_3}{\partial X} + \frac{dU_0}{\partial y}V_4 - \frac{\partial^2 U_2}{\partial X^2} + U_1\frac{\partial U_2}{\partial X} + U_2\frac{\partial U_1}{\partial X} + V_2\frac{\partial U_2}{\partial y} + V_3\frac{\partial U_1}{\partial y}, \tag{A11a}$$

$$\frac{\partial V_4}{\partial y} = -\frac{\partial U_3}{\partial X}, \quad \frac{\partial P_3}{\partial y} = \frac{\partial^2 V_3}{\partial y^2} - U_0\frac{\partial V_2}{\partial X} + \mathrm{Pr}^{-1}\Theta_3, \tag{A11b,c}$$

$$\frac{\partial^2 \Theta_4}{\partial y^2} = \mathrm{Pr}U_0\frac{\partial \Theta_3}{\partial X} - \frac{\partial^2 \Theta_2}{\partial X^2} + \mathrm{Pr}\left[U_1\frac{\partial \Theta_2}{\partial X} + V_2\frac{\partial \Theta_2}{\partial y} + U_2\frac{\partial \Theta_1}{\partial X} + V_3\frac{\partial \Theta_1}{\partial y} + U_3\frac{\partial \Theta_0}{\partial X} + V_4\frac{\partial \Theta_0}{\partial y}\right], \tag{A11d}$$

$$U_4(X,\pm1) = 0, \quad V_4(X,\pm1) = 0, \quad \Theta_4(X,\pm1) = 0, \quad \left.\frac{\partial P_3}{\partial X}\right|_{\mathrm{mean}} = 0. \tag{A11e–h}$$

The pressure gradient term in (A11a) is purely periodic due to constraint (A11h). The remaining terms on the right-hand side of (A11a) produce an aperiodic component of U_4 in the form

$$U_{4,\mathrm{aper}}(X,y) = \mathrm{Pr}^{-2}\mathrm{Re}\ \mathrm{Ra}_p^2[L_{U41}(y) + \mathrm{Pr}\ L_{U42}(y)], \tag{A12}$$

which leads to the change of the driving force as well as the flow rate pulled by the plate of the form

$$\Delta F_4 = -\frac{(2076\ +\ 13\,375\,\mathrm{Pr})}{17\,027\,010\,000}\mathrm{Re}\,\mathrm{Pr}^2\,\mathrm{Ra}_p^2\ , \quad \Delta Q_4 = \frac{(92\ +\ 83\,\mathrm{Pr})}{681\,080\,400}\mathrm{Re}\,\mathrm{Pr}^2\,\mathrm{Ra}_p^2\ . \tag{A13a,b}$$

The right-hand terms of (A11d) produce an aperiodic component of Θ_4 of the form

$$\Theta_{4,\mathrm{aper}}(X,y) = \mathrm{Ra}_p^2[L_{\Theta41}(y) + \mathrm{Ra}_{\mathrm{uni}}L_{\Theta42}(y) + \mathrm{Re}^2 L_{\Theta43}(y)], \tag{A14}$$

which gives rise to a heat flux

$$\mathrm{Nu}_{\mathrm{av},4} = -\frac{\mathrm{Ra}_p^2}{34\,054\,020\,000}[14\,774\,760 - 149\,148\mathrm{Ra}_{\mathrm{uni}} + (52\,014 + 82\,200\mathrm{Pr} + 367\,655\mathrm{Pr}^2)\mathrm{Re}^2]. \tag{A15}$$

Coefficients L_{U41}, L_{U42}, L_{Q41}, ..., L_{Q43} in the above are not given due to excessive length. The final expressions for the quantities of interest are

$$\Delta F = -\alpha^4 \frac{(2076 + 13\,375\,\mathrm{Pr})}{170\,27\,010\,000}\mathrm{Re}\,\mathrm{Pr}^2\mathrm{Ra}_p^2 + O(\alpha^5),$$
$$\Delta Q = \alpha^4 \frac{(92 + 83\,\mathrm{Pr})}{681\,080\,400}\mathrm{Re}\,\mathrm{Pr}^2\mathrm{Ra}_p^2 + O(\alpha^5),$$
$$\mathrm{Nu}_{av} = \frac{1}{2}\mathrm{Ra}_{\mathrm{uni}} + \frac{1}{1400}\alpha^2\mathrm{Ra}_p^2 + \alpha^4\mathrm{Nu}_{av,4} + O(\alpha^5). \tag{A16}$$

Equation (A13) demonstrates that periodic heating always decreases the force and increases the flow rate driven by the upper plate while the uniform heating plays no role in these processes. The heating creates periodic modulations of the flow and temperature fields [Eq. (A6)]. Interactions between the conductive and convective modulations create a net heat flow between the plates at $O(\alpha^2)$ and additional periodic modulations of the velocity and temperature fields [Eq. (A8)]. Further modulations are added at $O(\alpha^3)$. Finally, the nonlinear interactions between the velocity field modulations at $O(\alpha^4)$ change the driving force as well as the flow rate driven by the motion of the plate. This suggests that the largest heat flow will occur for α producing the most effective interactions between the conductive temperature modulations and the primary flow field modulations. The largest force reduction will occur for α leading to the most effective nonlinear interactions between the flow field modulations. These two α's are not the same.

APPENDIX B: SHORT-WAVELENGTH HEATING ($\alpha \to \infty$)

This analysis is focused on periodic heating only. The flow variables are decomposed into the isothermal flow identified using subscript 0 and modifications due to heating identified using subscript 1, and the temperature field is separated into the conductive field θ_0 and convective modifications θ_1:

$$u = u_0 + u_1, \quad v = v_1, \quad p = p_1, \quad \theta = \theta_0 + \theta_1, \tag{B1a}$$

where u, u_1 and v are scaled using $U_v{}^* = \nu^*/h^*$, u_0 is scaled using U^*_{top}, p is scaled using $\rho^* U_v^{*2}$, θ and θ_1 are scaled using $\nu^*\kappa^*/(g^*\,\Gamma^*\,h^{*3})$, and

$$u_0 = \frac{\mathrm{Re}}{2}(1+y), \quad \theta_0 = \frac{\mathrm{Ra}_p}{4}\left[\frac{\cosh(\alpha y)}{\cosh(\alpha)} - \frac{\sinh(\alpha y)}{\sinh(\alpha)}\right]\cos(\alpha x). \tag{B1b,c}$$

The conductive temperature field can be approximated in the limit of $\alpha \to \infty$ as

$$\theta_0 = \frac{\mathrm{Ra}_p}{2}\,[e^{-\alpha(1+y)} + O(e^{-\alpha})]\cos(\alpha x), \tag{B2}$$

which demonstrates the formation of a thermal boundary layer near the heated wall. Introduce the fast scale $\xi = \alpha x$ in the horizontal direction and the stretched scale $\eta = \alpha(1+y)$ in the vertical direction, and represent the inner solution as expansions of the form

$$[u_{1,in}(\xi,\eta), v_{1,in}(\xi,\eta), \theta_{1,in}(\xi,\eta)] = \sum_{n=2}^{n=7} \alpha^{-n}[U_n(\xi,\eta), V_n(\xi,\eta), \Theta_n(\xi,\eta)] + O(\alpha^{-8}), \tag{B2a}$$

$$[p_{1,in}(\xi,\eta)] = \sum_{n=1}^{n=6} \alpha^{-n}[P_n(\xi,\eta)] + O(\alpha^{-7}). \tag{B2b}$$

The flow properties of interest are expressed as similar expansions:

$$\Delta F = \sum_{n=2}^{n=7} \Delta F_n\,\alpha^{-n}, \quad \Delta Q = \sum_{n=2}^{n=7} \Delta Q_n\,\alpha^{-n}, \quad \mathrm{Nu}_{av} = \sum_{n=2}^{n=7} \mathrm{Nu}_{av,n}\,\alpha^{-n}. \tag{B3a–c}$$

Substitution of (B2) into the field equations and grouping terms of the same orders of magnitude result in the following systems and their solutions:

$$O(\alpha^{-2}) \ : \ \frac{\partial^2 U_2}{\partial \xi^2}+\frac{\partial^2 U_2}{\partial \eta^2}-\frac{\partial P_1}{\partial \xi}=0, \quad \frac{\partial^2 V_2}{\partial \xi^2}+\frac{\partial^2 V_2}{\partial \eta^2}-\frac{\partial P_1}{\partial \eta}=-\frac{\mathrm{Ra}_p}{2\,\mathrm{Pr}}e^{-\eta}\cos(\xi), \tag{B4a,b}$$

$$\frac{\partial U_2}{\partial \xi}+\frac{\partial V_2}{\partial \eta}=0, \quad \frac{\partial^2 \Theta_2}{\partial \xi^2}+\frac{\partial^2 \Theta_2}{\partial \eta^2}=-\frac{1}{4}\,\mathrm{Pr}\,\mathrm{Ra}_p\,\mathrm{Re}\,\eta e^{-\eta}\sin(\xi), \tag{B4c,d}$$

$$U_2(0)=0, \quad V_2(0)=0, \quad \Theta_2(0)=0, \quad \left.\frac{\partial P_2}{\partial \xi}\right|_{\mathrm{mean}}=0, \tag{B4e}$$

$$U_2(\xi,\eta)=\frac{\mathrm{Ra}_p}{16\,\mathrm{Pr}}\eta(-2+\eta)e^{-\eta}\sin(\xi), \quad V_2(\xi,\eta)=\frac{\mathrm{Ra}_p}{16\,\mathrm{Pr}}\eta^2 e^{-\eta}\cos(\xi), \tag{B5a,b}$$

$$\Theta_2(\xi,\eta)=\frac{\mathrm{Ra}_p}{16\mathrm{Pr}}\mathrm{Re}\,\eta(1+\eta)e^{-\eta}\sin(\xi). \quad \Delta F_2=0, \quad \Delta Q_2=0, \quad \mathrm{Nu}_{av,2}=0, \tag{B5c–f}$$

$$O(\alpha^{-3}) \ : \ \frac{\partial^2 U_3}{\partial \xi^2}+\frac{\partial^2 U_3}{\partial \eta^2}-\frac{\partial P_2}{\partial \xi}=0, \quad \frac{\partial^2 V_3}{\partial \xi^2}+\frac{\partial^2 V_3}{\partial \eta^2}-\frac{\partial P_2}{\partial \eta}=0, \quad \frac{\partial U_3}{\partial \xi}+\frac{\partial V_3}{\partial \eta}=0, \tag{B6a–c}$$

$$\frac{\partial^2 \Theta_3}{\partial \xi^2}+\frac{\partial^2 \Theta_3}{\partial \eta^2}=-\frac{1}{2}\mathrm{Pr}\,\mathrm{Ra}_p[U_2 e^{-\eta}\,\sin(\xi)\,-V_2 e^{-\eta}\,\cos(\xi)], \tag{B6d}$$

$$U_3(0)=0, \ V_3(0)=0, \quad \Theta_3(0)=0, \quad \left.\frac{\partial P_3}{\partial \xi}\right|_{\mathrm{mean}}=0, \tag{B6e}$$

$$U_3(\xi,\eta)=0, \quad V_3(\xi,\eta)=0, \tag{B7a,b}$$

$$\Theta_3(\xi,\eta)=\frac{\mathrm{Ra}_p^2}{256}+C_1\,\eta-\frac{\mathrm{Ra}_p^2}{128}\left(\frac{1}{2}+\eta+\eta^2\right)e^{-2\eta}+\frac{\mathrm{Ra}_p^2}{512}\eta(1+2\eta)\cos(2\xi), \tag{B7c}$$

$$\Delta F_3=0, \quad \Delta Q_3=0, \quad \mathrm{Nu}_{av,3}=C_1. \tag{B7d–f}$$

Θ_3 has an aperiodic part [the first three terms in (B7c)] which generates a heat flow from the lower to the upper wall, and C_1 is a constant which needs to be determined by matching with the outer solution:

$$O(\alpha^{-4}): \frac{\partial^2 U_4}{\partial \xi^2}+\frac{\partial^2 U_4}{\partial \eta^2}-\frac{\partial P_3}{\partial \xi}=\frac{\mathrm{Re}}{2}\eta\frac{\partial U_2}{\partial \xi}+\frac{\mathrm{Re}}{2}V_2\,, \quad \frac{\partial^2 V_4}{\partial \xi^2}+\frac{\partial^2 V_4}{\partial \eta^2}\,-\frac{\partial P_3}{\partial \eta}=\frac{\mathrm{Re}}{2}\eta\frac{\partial V_2}{\partial \xi}-\frac{\Theta_2}{Pr}, \tag{B8a,b}$$

$$\frac{\partial U_4}{\partial \xi}+\frac{\partial V_4}{\partial \eta}=0, \quad \frac{\partial^2 \Theta_4}{\partial \xi^2}+\frac{\partial^2 \Theta_4}{\partial \eta^2}=\frac{1}{2}\,\mathrm{Pr}\,\mathrm{Re}\,\eta\frac{\partial \Theta_2}{\partial \xi}, \tag{B8c,d}$$

$$U_4(0)=0, \ V_4(0)=0, \quad \Theta_4(0)=0, \quad \left.\frac{\partial P_4}{\partial \xi}\right|_{\mathrm{mean}}=0, \tag{B8e}$$

$$U_4(\xi,\eta)=\frac{1}{768\,\mathrm{Pr}}\mathrm{Ra}_p\,Re[(-24-6\eta-\eta^2+\eta^3)+\mathrm{Pr}(-30-3\eta+2\eta^2+\eta^3)]\,\eta e^{-\eta}\cos(\xi), \tag{B9a}$$

$$V_4(\xi,\eta)=\frac{1}{768\,\mathrm{Pr}}\mathrm{Ra}_p\,\mathrm{Re}[(12+6\eta+2\eta^2)+\mathrm{Pr}(15+6\eta+\eta^2)]\eta^2 e^{-\eta}\sin(\xi), \tag{B9b}$$

$$\Theta_4(\xi,\eta)=-\frac{1}{768}\mathrm{Pr}^2\mathrm{Ra}_p\mathrm{Re}^2\,\eta(15+15\eta+10\eta^2+3\eta^3)e^{-\eta}\cos(\xi), \tag{B9c}$$

$$\Delta F_4=0, \quad \Delta Q_4=0, \quad \mathrm{Nu}_{av,4}=0, \tag{B9d–f}$$

$$O(\alpha^{-5}):\ \frac{\partial^2 U_5}{\partial \xi^2}+\frac{\partial^2 U_5}{\partial \eta^2}-\frac{\partial P_4}{\partial \xi}=\frac{\mathrm{Re}}{2}\eta\frac{\partial U_3}{\partial \xi}+U_2\frac{\partial U_2}{\partial \xi}+V_2\frac{\partial U_2}{\partial \eta}+\frac{\mathrm{Re}}{2}V_3, \tag{B10a}$$

$$\frac{\partial^2 V_5}{\partial \xi^2}+\frac{\partial^2 V_5}{\partial \eta^2}-\frac{\partial P_4}{\partial \eta}=\frac{\mathrm{Re}}{2}\eta\frac{\partial V_3}{\partial \xi}+U_2\frac{\partial V_2}{\partial \xi}+V_2\frac{\partial V_2}{\partial \eta}-\frac{\Theta_3}{\mathrm{Pr}},\quad \frac{\partial U_5}{\partial \xi}+\frac{\partial V_5}{\partial \eta}=0, \tag{B10b,c}$$

$$\frac{\partial^2 \Theta_5}{\partial \xi^2}+\frac{\partial^2 \Theta_5}{\partial \eta^2}$$
$$=\mathrm{Pr}\left[\frac{1}{2}\mathrm{Re}\,\eta\frac{\partial \Theta_3}{\partial \xi}+U_2\frac{\partial \Theta_2}{\partial \xi}-\frac{1}{2}U_4\mathrm{Ra}_p\,e^{-\eta}\sin(\xi)+V_2\frac{\partial \Theta_2}{\partial \eta}-\frac{1}{2}\,V_4\mathrm{Ra}_p\,e^{-\eta}\cos(\xi)\right], \tag{B10d}$$

$$U_5(0)=0,\ V_5(0)=0,\ \Theta_5(0)=0,\quad \left.\frac{\partial P_5}{\partial \xi}\right|_{\mathrm{mean}}=0, \tag{B10e}$$

$$U_5(\xi,\eta)=\frac{1}{49\,152\,\mathrm{Pr}^2}\,\mathrm{Ra}_p^2\,[3-3\eta-8\eta^2+4\eta^3+\mathrm{Pr}(-15-3\eta+4\eta^2+4\eta^3)]\,\eta e^{-2\eta}\sin(2\xi), \tag{B11a}$$

$$V_5(\xi,\eta)=\frac{1}{49\,152\,\mathrm{Pr}^2}\mathrm{Ra}_p^2\,[-3+4\eta^2+\mathrm{Pr}(15+12\eta+4\eta^2)]\,\eta^2 e^{-2\eta}\cos(2\xi), \tag{B11b}$$

$$\Theta_5(\xi,\eta)=\frac{1}{49\,152}\mathrm{Ra}_p^2\,\mathrm{Re}[36+72\eta+32\eta^2+8\eta^3+\mathrm{Pr}(51+102\eta+56\eta^2+16\eta^3)]\eta e^{-2\eta}\sin(2\xi), \tag{B11c}$$

$$\Delta F_5=0,\quad \Delta Q_5=0,\quad \mathrm{Nu}_{av,5}=0, \tag{B11d–f}$$

$$O(\alpha^{-6}):\ \frac{\partial^2 U_6}{\partial \xi^2}+\frac{\partial^2 U_6}{\partial \eta^2}-\frac{\partial P_5}{\partial \xi}=\frac{\mathrm{Re}}{2}\eta\frac{\partial U_4}{\partial \xi}+\frac{\mathrm{Re}}{2}V_4,\quad \frac{\partial^2 V_6}{\partial \xi^2}+\frac{\partial^2 V_6}{\partial \eta^2}-\frac{\partial P_5}{\partial \eta}=\frac{\mathrm{Re}}{2}\eta\frac{\partial V_4}{\partial \xi}-\frac{\Theta_4}{\mathrm{Pr}}, \tag{B12a,b}$$

$$\frac{\partial U_6}{\partial \xi}+\frac{\partial V_6}{\partial \eta}=0, \tag{B12c}$$

$$\frac{\partial^2 \Theta_6}{\partial \xi^2}+\frac{\partial^2 \Theta_6}{\partial \eta^2}$$
$$=\mathrm{Pr}\left[\frac{1}{2}\mathrm{Re}\,\eta\frac{\partial \Theta_4}{\partial \xi}+U_2\frac{\partial \Theta_3}{\partial \xi}+V_2\frac{\partial \Theta_3}{\partial \eta}-\frac{1}{2}U_5\mathrm{Ra}_p e^{-\eta}\sin(\xi)-\frac{1}{2}\,V_5\mathrm{Ra}_p e^{-\eta}\cos(\xi)\right], \tag{B12d}$$

$$U_6(0)=0,\ V_6(0)=0,\ \Theta_6(0)=0,\quad \left.\frac{\partial P_6}{\partial \xi}\right|_{\mathrm{mean}}=0, \tag{B12e}$$

$$U_6(\xi,\eta)=\frac{\mathrm{Ra}_p\mathrm{Re}^2}{92\,160\,\mathrm{Pr}}[2250+720\eta+345\eta^2+45\eta^3-9\eta^4-8\eta^5+\mathrm{Pr}(2070+630\eta$$
$$+285\eta^2-18\eta^4-4\eta^5)-3\mathrm{Pr}^2(-900-180\eta-30\eta^2+5\eta^3+5\eta^4+\eta^5)]\eta e^{-\eta}\sin(\xi), \tag{B13a}$$

$$V_6(\xi,\eta)=-\frac{\mathrm{Ra}_p\mathrm{Re}^2}{92\,160\,\mathrm{Pr}}[1125+615\eta+240\eta^2+57\eta^3+8\eta^4+\mathrm{Pr}(1035+555\eta$$
$$+210\eta^2+42\eta^3+4\eta^4)+3\mathrm{Pr}^2(450+210\eta+60\eta^2+11\eta^3+\eta^4)]\eta^2 e^{-\eta}\cos(\xi), \tag{B13b}$$

$$\Theta_6(\xi,\eta)=\frac{Ra_p}{21\,233\,664\ Pr}\Bigg\{-27\Bigg[4096\ C_1\,\mathrm{Pr}\,\eta(3+3\eta+2\eta^2)e^{2\eta}$$
$$+\frac{\mathrm{Ra}_p^2}{4}((-18+843\,\mathrm{Pr})e^{2\eta}+\ 2(9+18\eta+18\eta^2+16\eta^3+8\eta^4)-\mathrm{Pr}(843+1584\eta$$
$$+1380\eta^2+688\eta^3+\ 176\eta^4))\Bigg]\cos(\xi)+\mathrm{Ra}_p^2\big[-5-15\eta+24\eta^2+36\eta^3$$
$$+\ \mathrm{Pr}\left(127+381\eta+492\eta^2+\ 252\eta^3\right)\big]\eta\ \cos(3\xi)-\ 3456\,\mathrm{Pr}^4\mathrm{Re}^3\ \eta(90+90\eta+60\eta^2$$
$$+25\eta^3+7\eta^4+\ \eta^5)e^{2\eta}\sin(\xi)\Bigg\}e^{-3\eta}, \tag{B13c}$$

$$\Delta F_6=0,\quad \Delta Q_6=0,\quad \mathrm{Nu}_{av,6}=0, \tag{B13d–f}$$

$$O(\alpha^{-7}):\ \frac{\partial^2U_7}{\partial\xi^2}+\frac{\partial^2U_7}{\partial\eta^2}-\frac{\partial P_6}{\partial\xi}=\frac{\mathrm{Re}}{2}\eta\frac{\partial U_5}{\partial\xi}+\frac{\mathrm{Re}}{2}V_5+U_2\frac{\partial U_4}{\partial\xi}+U_4\frac{\partial U_2}{\partial\xi}+V_2\frac{\partial U_4}{\partial\eta}+V_4\frac{\partial U_2}{\partial\eta}, \tag{B14a}$$

$$\frac{\partial^2V_7}{\partial\xi^2}+\frac{\partial^2V_7}{\partial\eta^2}-\frac{\partial P_6}{\partial\eta}=\frac{\mathrm{Re}}{2}\eta\frac{\partial V_5}{\partial\xi}+U_2\frac{\partial V_4}{\partial\xi}+U_4\frac{\partial V_2}{\partial\xi}+V_2\frac{\partial V_4}{\partial\eta}+V_4\frac{\partial V_2}{\partial\eta}-\frac{\Theta_5}{\mathrm{Pr}}, \tag{B14b}$$

$$\frac{\partial U_7}{\partial\xi}+\frac{\partial V_7}{\partial\eta}=0, \tag{B14c}$$

$$\frac{\partial^2\Theta_7}{\partial\xi^2}+\frac{\partial^2\Theta_7}{\partial\eta^2}=\mathrm{Pr}\Bigg[\frac{1}{2}\mathrm{Re}\ \eta\frac{\partial\Theta_5}{\partial\xi}+U_2\frac{\partial\Theta_4}{\partial\xi}+V_2\frac{\partial\Theta_4}{\partial\eta}+U_4\frac{\partial\Theta_2}{\partial\xi}+V_4\frac{\partial\Theta_2}{\partial\eta}$$
$$-\frac{1}{2}U_6\mathrm{Ra}_pe^{-\eta}\sin(\xi)-\frac{1}{2}\ V_6\mathrm{Ra}_pe^{-\eta}\cos(\xi)\Bigg], \tag{B14d}$$

$$U_7(0)=0,\ V_7(0)=0,\ \Theta_7(0)=0,\quad \left.\frac{\partial P_7}{\partial\xi}\right|_{\mathrm{mean}}=0. \tag{B14e}$$

Equation (B14a) dictates that the last four terms on the RHS are aperiodic, and the corresponding aperiodic parts of the solution $U_{7,ap}$ and $V_{7,ap}$ can easily be determined:

$$U_{7,ap}(\eta)=C_2\ \eta+\frac{\mathrm{Ra}_p^2\ \mathrm{Re}}{98\,304\mathrm{Pr}^2}[(48+33\mathrm{Pr})-\{\ L_{71}(\eta)+\mathrm{Pr}\ \ L_{72}(\eta)\}\mathrm{e}^{-2\eta}],\quad V_{7,ap}(\eta)=0, \tag{B15a,b}$$

where $L_{71}(\eta)=8(6+12\eta+12\eta^2+8\eta^3+4\eta^4+\eta^5)$, $L_{72}(\eta)=33+66\eta+66\eta^2+44\eta^3+22\eta^4+4\eta^5$ and the constant C_2 needs to be determined by matching with the outer solution.

The outer solution has the following form:

$$u_{1,\mathrm{out}}(x,y)=\alpha^{-7}\ \hat{U}_7(y)+O(\alpha^{-8}),\quad v_{1,\mathrm{out}}(x,y)=0, \tag{B16a}$$

$$p_{1,\mathrm{out}}(x,y)=\alpha^{-3}\ \hat{P}_3(y)+O(\alpha^{-8}),\quad \theta_{1,\mathrm{out}}(x,y)=\alpha^{-3}\ \hat{\Theta}_3(y)+O(\alpha^{-8}). \tag{B16b}$$

Substitution of (B16) into the field equations and retention of the leading-order terms result in the following system:

$$\frac{\partial^2\hat{U}_7}{\partial y^2}=0,\quad \frac{\partial\hat{P}_3}{\partial y}=\mathrm{Pr}^{-1}\ \hat{\Theta}_3,\quad \frac{\partial^2\hat{\Theta}_3}{\partial y^2}=0, \tag{B17a–c}$$

$$\hat{U}_7(x,1)=0,\quad \hat{\Theta}_3(x,1)=0,\quad \left.\frac{\partial\hat{P}_3}{\partial X}\right|_{\mathrm{mean}}=0, \tag{B17d–f}$$

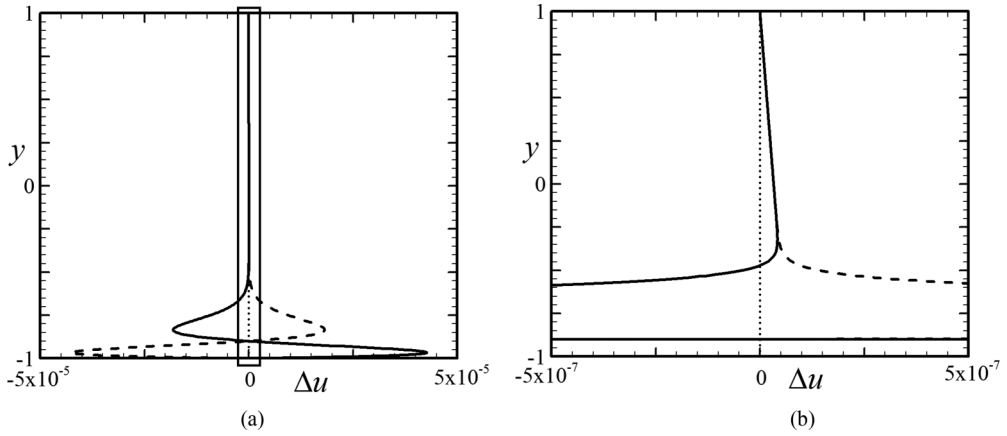

FIG. 24. Variations of the difference between the actual and the isothermal x-velocity components, $\Delta u(=u - u_{\rm iso})$, as functions of y for $\mathrm{Ra}_P = 1000$, $\mathrm{Re} = 1$, $\mathrm{Pr} = 0.71$, $\mathrm{Ra}_{\rm uni} = 0$, $\alpha = 30$, at $x/\lambda = 0$ (solid line) and $x/\lambda = 0.5$ (dashed line). Enlargement of the box shown in panel (a) is displayed in panel (b).

whose solution has the following form:

$$\hat{U}_7(y) = \hat{A}_7(y-1), \quad \hat{P}_3(y) = \hat{A}_3(y^2/2 - y), \quad \hat{\Theta}_3(y) = \hat{A}_3(y-1). \tag{B18a–c}$$

Matching of (B18) with (B15a) and (B7c) leads to the determination of constants $\hat{A}_7$, $\hat{A}_3$ and the composite solution expressed in terms of the outer variable in the form

$$u_{1,ap}(y) = \alpha^{-7}\left\{\frac{\mathrm{Ra}_p^2 \mathrm{Re}}{98\,304\,\mathrm{Pr}^2}\left[\frac{1}{2}(48+33\,\mathrm{Pr})(1-y) - (L_{71} + \mathrm{Pr}\,L_{72})\alpha(1+y)\mathrm{e}^{-2\alpha(1+y)}\right]\right\} + O(\alpha^{-8}), \tag{B19a}$$

$$\Theta(x,y) = \alpha^{-3}\left\{\begin{array}{c}\frac{\mathrm{Ra}_p^2}{256}(1-y) - \frac{\mathrm{Ra}_p^2}{128}\left[\frac{1}{2} + \alpha(1+y) + \alpha^2(1+y)^2\right]e^{-2\alpha(1+y)} \\ + \frac{\mathrm{Ra}_p^2}{512}\left[\alpha(1+y) + 2\alpha^2(1+y)^2\right]\cos(2\alpha x)\end{array}\right\} + O(\alpha^{-5}). \tag{B19b}$$

Analysis of (B19a) shows that the edge of boundary layer appears to the external flow as a wall moving to the right adding a velocity correction linear in y (see Fig. 24). This is the mechanism through which the heating increases the overall flow rate and decreases the driving force. The edge of the boundary layer appears to the outer zone as a hot wall resulting in the formation of a temperature component linear in y (see Fig. 25). The split of the temperature field into a uniform, x-independent and conduction-dominated outer zone and a complex, convection-dominated boundary layer is clearly visible.

The final expressions for the force and flow rate corrections, and for the Nusselt number are

$$\Delta F = -\frac{16+11\mathrm{Pr}}{65\,536\,\mathrm{Pr}^2}\,\mathrm{Ra}_p^2\,\mathrm{Re}\,\alpha^{-7} + 0(\alpha^{-8}), \quad \Delta Q = \frac{61+41\mathrm{Pr}}{32\,768\,\mathrm{Pr}^2}\,\mathrm{Ra}_p^2\,\mathrm{Re}\,\alpha^{-7} + 0(\alpha^{-8}), \tag{B19c,d}$$

$$\mathrm{Nu}_{av} = \frac{\mathrm{Ra}_p^2}{512}\alpha^{-3} + 0(\alpha^{-8}). \tag{B19e}$$

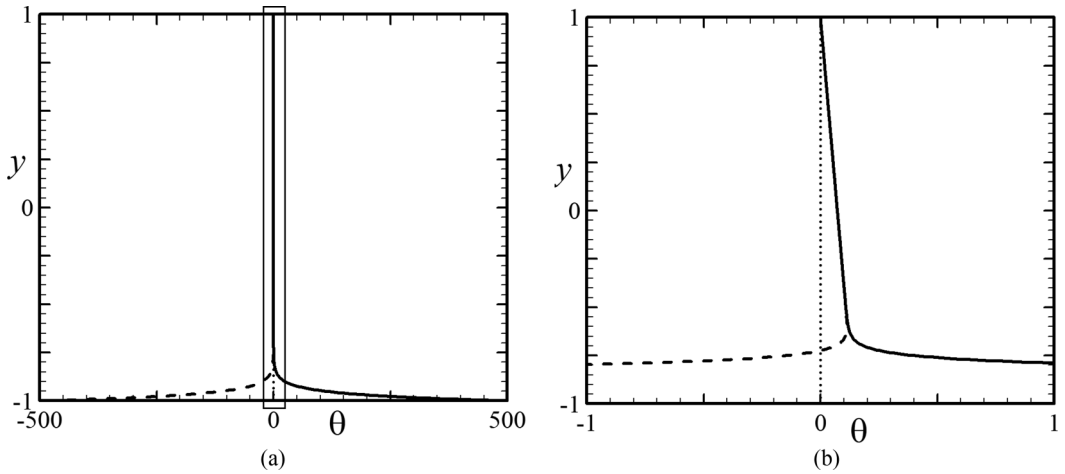

FIG. 25. Variations of the temperature θ as functions of y for $\mathrm{Ra}_P = 1000$, $\mathrm{Re} = 1$, $\mathrm{Pr} = 0.71$, $\mathrm{Ra}_{\mathrm{uni}} = 0$, $\alpha = 30$ at $x/\lambda = 0$ (solid line) and $x/\lambda = 0.5$ (dashed line). Enlargement of the box shown in panel (a) is displayed in panel (b).

[1] V. A. Romanow, Stability of plane-parallel Couette flow, Funct. Anal. Applics. **7**, 137 (1972).

[2] K. Deguchi and M. Nagata, Bifurcations and instabilities in sliding Couette flow, J. Fluid Mech. **678**, 156 (2011).

[3] J. M. Floryan, Centrifugal instability of Couette flow over a wavy wall, Phys. Fluids **14**, 312 (2002).

[4] H. V. Moradi and J. M. Floryan, Sliding Couette flow in a ribbed annulus, Phys. Fluids **28**, 074103 (2016).

[5] J. M. Floryan, Wall-transpiration-induced instabilities in plane Couette flow, J. Fluid Mech. **488**, 151 (2003).

[6] P. Gittler, Stability of Poiseuille–Couette flow between concentric cylinders, Acta Mech. **101**, 1 (1993).

[7] A. W. Ogunsola and B. A. Peter, Analytical solution of non-isothermal Couette flow between two plates, IOSR J. Math. **10**, 44 (2014).

[8] H. Bénard, Les tourbillons cellulaires dans une nappe liquide, Rev. Générale Sci. Pure Appl. **11**, 1261 (1900).

[9] J. W. S. Rayleigh, On convection currents in a horizontal layer of fluid, when the higher temperature is on the under side, Phil. Mag. **32**, 529 (1916).

[10] R. E. Kelly, The onset and development of thermal convection in fully developed shear flows, Adv. App. Mech. **31**, 35 (1994).

[11] M. Z. Hossain, D. Floryan, and J. M. Floryan, Drag reduction due to spatial thermal modulations, J. Fluid Mech. **713**, 398 (2012).

[12] D. Floryan and J. M. Floryan, Drag reduction in heated channels, J. Fluid Mech. **765**, 353 (2015).

[13] M. Z. Hossain and J. M. Floryan, Drag reduction in a thermally modulated channel, J. Fluid Mech. **791**, 122 (2016).

[14] M. J. Walsh, Drag characteristics of V-groove and transverse curvature riblets, in *Viscous Flow Drag Reduction*, edited by G. R. Hough, Progress in Astronautics and Aeronautics, Vol. 72 (AIAA, 1980), pp. 168–184.

[15] M. J. Walsh, Riblets as a viscous drag reduction technique, AIAA J. **21**, 485 (1983).

[16] A. Mohammadi and J. M. Floryan, Effects of longitudinal grooves on the Couette-Poiseuille flow, J. Theor. Comp. Fluid Mech. **28**, 549 (2014).

[17] M. Z. Hossain and J. M. Floryan, Instabilities of natural convection in a periodically heated layer, J. Fluid Mech. **733**, 33 (2013).
[18] M. Z. Hossain and J. M. Floryan, Natural convection under sub-critical conditions in the presence of heating non-uniformities, Intl. J. Heat Mass Transfer **114**, 8 (2017).
[19] M. Z. Hossain and J. M. Floryan, Mixed convection in a periodically heated channel, J. Fluid Mech. **768**, 51 (2015).
[20] M. Z. Hossain and J. M. Floryan, Natural convection in a fluid layer periodically heated from above, Phys. Rev. E **90**, 023015 (2014).